



ELSEVIER

Available online at www.sciencedirect.com

Geochimica et Cosmochimica Acta xxx (2006) xxx–xxx

Geochimica

www.elsevier.com/locate/gca

$^{228}\text{Ra}/^{226}\text{Ra}$ and $^{226}\text{Ra}/\text{Ba}$ ratios to track barite formation and transport in the water column

P. van Beek^{a,*}, R. François^{b,c}, M. Conte^{b,d}, J.-L. Reyss^e, M. Souhaut^a, M. Charette^b

^a LEGOS, Laboratoire d'Etudes en Géophysique et Océanographie Spatiales (CNRS/CNES/IRD/IUPS), Observatoire Midi Pyrénées, 14 avenue Edouard Belin, 31400 Toulouse, France

^b Woods Hole Oceanographic Institution, Woods Hole, MA 02543, USA

^c University of British Columbia, Earth and Ocean Sciences Department, Vancouver, BC, Canada

^d Bermuda Biological Station for Research, Inc., Ferry Reach, St. Georges GE01, Bermuda

^e Laboratoire des Sciences du Climat et de l'Environnement, 91198 Gif-sur-Yvette, France

Received 3 November 2005; accepted in revised form 12 July 2006

14 Abstract

We measured $^{228}\text{Ra}_{\text{ex}}/^{226}\text{Ra}_{\text{ex}}$ and $^{226}\text{Ra}_{\text{ex}}/\text{Ba}_{\text{ex}}$ ratios in suspended and sinking particles collected at the Oceanic Flux Program (OFP) time-series site in the western Sargasso Sea and compared them to seawater ratios to provide information on the origin and transport of barite (BaSO_4) in the water column. The $^{228}\text{Ra}_{\text{ex}}/^{226}\text{Ra}_{\text{ex}}$ ratios of the suspended particles down to 2000 m are nearly identical to those of seawater at the same water depth. These ratios are much lower than expected if suspended barite was produced in surface waters and indicates that barite is produced throughout the mesopelagic layer. The $^{228}\text{Ra}_{\text{ex}}/^{226}\text{Ra}_{\text{ex}}$ activity ratios of sinking particles collected at 1500 and 3200 m varied mostly between 0.1 and 0.2, which is intermediate between the seawater ratio at these depths (<0.03) and the seawater ratios found in the upper 250 m (0.31–0.42). This suggests that excess Ba (i.e., $\text{Ba}_{\text{ex}} = \text{Ba}_{\text{total}} - \text{Ba}_{\text{lithogenic}}$), considered to be mainly barite, present in the sinking flux is a mixture of crystals formed recently in the upper water column, formed several years earlier in the upper water column, or formed recently in deeper waters. We observe a sizeable temporal variability in the $^{228}\text{Ra}_{\text{ex}}/^{226}\text{Ra}_{\text{ex}}$ ratios of sinking particles, which indicates temporal variability in the relative proportion of barite crystals originating from surface (with a high $^{228}\text{Ra}_{\text{ex}}/^{226}\text{Ra}_{\text{ex}}$ ratio) and mesopelagic (with a low $^{228}\text{Ra}_{\text{ex}}/^{226}\text{Ra}_{\text{ex}}$ ratio) sources. However, we could not discern a clear pattern that would elucidate the factors that control this variability. The $^{226}\text{Ra}/\text{Ba}$ ratios measured in seawater are consistent with the value reported from the GEOSECS expeditions ($2.3 \text{ dpm } \mu\text{mol}^{-1}$) below 500 m depth, but are significantly lower in the upper 500 m. High $^{226}\text{Ra}_{\text{ex}}/\text{Ba}_{\text{ex}}$ ratios and elevated Sr concentrations in suspended particles from the upper water column suggest preferential uptake of ^{226}Ra over Ba during formation of SrSO_4 skeletons by acantharians, which must contribute to barite formation in shallow waters. Deeper in the water column the $^{226}\text{Ra}_{\text{ex}}/\text{Ba}_{\text{ex}}$ ratios of suspended particles are lower than those of seawater. Since $^{228}\text{Ra}_{\text{ex}}/^{226}\text{Ra}_{\text{ex}}$ ratios demonstrate that suspended barite at these depths has been produced recently and in situ, their low $^{226}\text{Ra}_{\text{ex}}/\text{Ba}_{\text{ex}}$ ratios indicate preferential uptake of Ba over Ra in barite formed in mesopelagic water.

© 2006 Published by Elsevier Inc.

35 1. Introduction

Radium isotopes (^{228}Ra , $T_{1/2} = 5.75$ years, and ^{226}Ra , $T_{1/2} = 1602$ years) and barium (Ba) have been widely used to study ocean circulation and marine biogeochemical cycling. The global oceanic distribution of these elements

and isotopes was first documented during the GEOSECS program (Broecker et al., 1967, 1976; Wolgemuth and Broecker, 1970; Bacon and Edmond, 1972; Li et al., 1973; Chan et al., 1976; Ku and Lin, 1976; Chung and Craig, 1980; Ku et al., 1980). Water column profiles of ^{226}Ra and Ba show a similar depletion in surface water and increasing deep water concentrations from the Atlantic to the Pacific Ocean. This similarity between ^{226}Ra and Ba water column profiles was attributed to the nearly identical chemical properties of the two elements (Wolgemuth and

* Corresponding author. Fax: +33 5 61 25 32 05.

E-mail address: vanbeek@notos.cst.cnes.fr (P. van Beek).

50 Broecker, 1970). ^{226}Ra and Ba thus show a general linear
51 correlation over much of the water column in the Atlantic,
52 Antarctic and Pacific Oceans, with the result that the
53 $^{226}\text{Ra}/\text{Ba}$ ratio is fairly constant in the ocean (Li et al.,
54 1973; Chan et al., 1976; Ku et al., 1980; Foster et al.,
55 2004). Based on data from the Atlantic and Pacific Oceans,
56 Chan et al. (1976) estimated this ratio at 4.6 nmol $^{226}\text{Ra}/$
57 mol Ba (i.e., 2.3 dpm μmol^{-1}), similar to the ratios report-
58 ed in other places of the world (Li et al., 1973; Ku et al.,
59 1980; Foster et al., 2004). In near-bottom waters, however,
60 the correlation breaks down, with ^{226}Ra activities being
61 higher than those predicted from the radium-barium corre-
62 lation because of the input of ^{226}Ra from deep-sea sedi-
63 ments (Chung, 1974; Chan et al., 1976; Chung and Craig,
64 1980; Ku et al., 1980; Rhein and Schlitzer, 1988). This effect
65 is particularly pronounced in the deep-northeast Pacific
66 (Chan et al., 1974; Chung, 1976).

67 In contrast to ^{226}Ra , dissolved ^{228}Ra activities are high-
68 est in the upper water column and decrease rapidly through
69 the permanent pycnocline (Kaufman et al., 1973; Li et al.,
70 1980; Moore, 1987). The high ^{228}Ra activities in the upper
71 water column and deep waters reflect lateral transport of
72 ^{228}Ra that diffused from shelf sediments and release from
73 deep-sea sediments, respectively. The low activities in inter-
74 mediate waters reflect the slow vertical mixing compared to
75 radioactive decay.

76 Surface depletion of Ba and ^{226}Ra results mainly from
77 barite precipitation in the upper water column (Chow
78 and Goldberg, 1960; Dehairs et al., 1980, 1990; Bishop,
79 1988; Stroobants et al., 1991). Since the world's oceans
80 were found to be mostly undersaturated with respect to
81 barite (Church and Wolgemuth, 1972), it was proposed
82 that barite precipitation takes place in the upper water col-
83 umn within supersaturated microenvironments that result
84 from the decay of organic matter (Chow and Goldberg,
85 1960; Dehairs et al., 1980; Bishop, 1988; Stroobants
86 et al., 1991; Ganeshram et al., 2003). The correlation of
87 particulate Ba flux and export flux of organic carbon
88 (Dymond et al., 1992; François et al., 1995) has led to
89 the use of barite accumulation rates in deep-sea sediments
90 for paleoproductivity reconstructions (Schmitz, 1987;
91 Gingele and Dahmke, 1994; Paytan et al., 1996a; Nürnberg
92 et al., 1997).

93 Additionally, it has been proposed that dissolution of
94 celestite (SrSO_4) skeletons made by acantharians and en-
95 riched in barium might contribute significantly to barite
96 formation (Bernstein et al., 1987, 1992, 1998; Bernstein
97 and Byrne, 2004). Acantharians are documented as ubiqui-
98 tous and abundant marine protozoans. Their presence is
99 especially well documented in the Sargasso Sea (Michaels,
100 1988; Michaels et al., 1995; Bernstein et al., 1992, 1998).
101 Acantharians are generally concentrated in surface waters
102 and their abundance rapidly decreases below 150 m be-
103 cause celestite rapidly dissolves after the death of the
104 organism (Bishop et al., 1977, 1978; Michaels, 1988; Mi-
105 chaels et al., 1995; Bernstein et al., 1992). Bernstein et al.
106 (1992) reported the presence of acantharians as deep as

400 m but specimen became very rare to non-existent in
their trap located at 1500 m. These authors also described
the presence of large number of cysts and minute SrSO_4
particles that could be related to the acantharian reproduc-
tive cycle. Because acantharians and acantharian-derived
particles are enriched in barium and are also expected to
incorporate radium, Bernstein et al. (1992, 1998) suggested
that acantharians might play a substantial role in oceanic
Ba and Ra cycling.

When barite precipitates, it acquires the $^{228}\text{Ra}/^{226}\text{Ra}$ ra-
tio of the ambient seawater at the time and depth of forma-
tion (Legeleux and Reyss, 1996). Legeleux and Reyss
(1996) compared the $^{228}\text{Ra}/^{226}\text{Ra}$ ratio of sinking particles
collected with sediment traps in the tropical northeast
Atlantic Ocean to that of seawater. From the sharp de-
crease in seawater $^{228}\text{Ra}/^{226}\text{Ra}$ ratio with depth, they ar-
gued that the relatively high $^{228}\text{Ra}/^{226}\text{Ra}$ measured in
deep sediment trap material indicated that most of the par-
ticulate Ba (presumably barite) is formed in the upper
250 m of the water column. Moore and Dymond (1991)
measured the $^{226}\text{Ra}/\text{Ba}$ ratio in sinking particles collected
in the equatorial Pacific and found that particles removed
 ^{226}Ra and Ba from waters in the upper water column with
a ratio similar to that of seawater. Also observed was a de-
crease in the $^{226}\text{Ra}/\text{Ba}$ ratios of particles with depth, which
they attributed to the presence of old barite crystals (with
low $^{226}\text{Ra}/\text{Ba}$ ratio due to ^{226}Ra decay) that were either lat-
erally transported from continental margins or resuspend-
ed from the seafloor by deep-sea currents.

The ^{226}Ra decay in barite accumulated in deep-sea sed-
iments has also been used to estimate Holocene sedimenta-
tion rates (Paytan et al., 1996b; van Beek and Reyss, 2001;
van Beek et al., 2002, 2004). Dating of marine carbonate
shells has also been attempted (Berkman and Ku, 1998;
Staubwasser et al., 2004). The latter method, however, re-
lies on knowing the initial $^{226}\text{Ra}/\text{Ba}$ ratio incorporated by
carbonates, which can be assumed to be 4.6 nmol $^{226}\text{Ra}/$
mol Ba or 2.3 dpm μmol^{-1} (that is, the seawater ratio
found to be fairly constant in the oceans; Chan et al.,
1976). Both applications require a better understanding
of the factors that control (i) the seawater Ba and ^{226}Ra
distributions and (ii) the incorporation of ^{226}Ra in particu-
late phases such as barite or carbonates.

Analysis of radium isotopes in a particulate Ba phase
such as barite can thus provide information on its origin
and flux in the water column and more generally on pro-
cesses such as advection, resuspension and isopycnal mix-
ing that influence the transport of suspended particles in
the ocean. In this study, we measured Ba concentrations,
 $^{226}\text{Ra}/\text{Ba}$ and $^{228}\text{Ra}/^{226}\text{Ra}$ ratios in seawater and in sus-
pended and sinking particles collected at the Oceanic Flux
Program (OFP) site in the western Sargasso Sea off Bermu-
da ($31^\circ 50' \text{N}$; $64^\circ 10' \text{W}$; 4500 m water depth) to track barite
formation and transport in the water column. To our
knowledge, this work reports the first ^{226}Ra and ^{228}Ra
activities measured in suspended particles. This allowed
us to combine seawater data with data from both the

164 sinking and suspended particle pools. Additionally, be-
165 cause previous studies reported abundant acantharian pop-
166 ulations in the Sargasso Sea, which might influence the Ba
167 and Ra distributions, Sr contents were analyzed in sus-
168 pended particles to track the presence of acantharians.

169 2. Materials and methods

170 2.1. Sample collection

171 The Oceanic Flux Program (OFP) sediment trap time-
172 series mooring (Conte et al., 2001) is located in the north-
173 ern Sargasso Sea in a transitional region between relatively
174 eutrophic waters to the north and oligotrophic subtropical
175 waters to the south. In addition to the OFP sediment trap
176 time-series, the area is the site of the Bermuda-Atlantic
177 Times Series (BATS, Steinberg et al., 2001) and the Bermu-
178 da testbed Mooring (BTM, Dickey et al., 2001).

179 Seawater samples were collected at the OFP site in May
180 2002 (from fourth to eighth) using a CTD equipped with
181 12-liter Niskin bottles. Sixty milliliter samples were collect-
182 ed for dissolved Ba measurements. For Ra isotopes, 50–
183 60 L of seawater was passed through a cartridge filled with
184 MnO_2 -coated fibers that retain radium isotopes (Moore
185 and Reid, 1973; Moore et al., 1985). The fibers were then
186 ashed (1 day at 820 °C) and transferred into counting vials
187 for gamma counting.

188 Suspended particles were collected using McLane large
189 volume in situ pumps (WTS, McLane Labs, Falmouth
190 Ma, USA). Up to 2300 L was filtered through 142-mm
191 diameter Versapor filters (acrylic copolymer on a nylon
192 substrate; Pall Corporation), with a pore size of 0.8 μm .

193 Sinking particles were collected using Parflux Mark VII
194 sediment traps (McLane Labs, Falmouth MA, USA). De-
195 tails of OFP sample collection and processing are given in
196 Conte et al. (2001). Sediment trap samples were analyzed
197 from both the 1500 and 3200 m depth traps. Analyses were
198 conducted on archived dried material collected in 1988–
199 1989 and 1999–2000. The integrated sampling period rang-
200 es between 58–76 days in 1988–1989 and 14–15 days in
201 1999–2000 (Table 3).

202 2.2. Analytical methods

203 2.2.1. Seawater

204 Seawater was analyzed for barium by isotope dilution
205 using a ^{135}Ba spike (precision: $\pm 2\%$ estimated from repli-
206 cate analyses), using the Inductively Coupled Plasma Mass
207 Spectrometry (ICP-MS) facility at Woods Hole Oceanog-
208 raphic Institution (Element, Finnigan). Radium isotopes
209 adsorbed on MnO_2 ash were counted at the underground
210 laboratory of Modane (Laboratoire Souterrain de Mod-
211 ane, French Alps). High-efficiency, low-background, well-
212 type germanium detectors (215, 430 and 950 cm^3) were
213 used (Reyss et al., 1995). These detectors are shielded from
214 cosmic radiation by 1700 m of rocks; a very low back-
215 ground is thus achieved, allowing the measurement of very

low activities. ^{226}Ra activities were determined using the
216 ^{214}Pb (295 and 352 keV) and ^{214}Bi (609 keV) peaks. ^{228}Ra
217 activities were determined using the 338, 911 and 969 keV
218 peaks of ^{228}Ac . Counting time for each sample ranges from
219 2 to 5 days. Uncertainties reported for ^{226}Ra and ^{228}Ra
220 activities are errors due to counting statistics. 221

222 2.2.2. Suspended particles

223 Results reported here for particles are based on bulk
224 analyses. Ra isotopes were first measured on intact filters
225 by gamma counting using the same method used for the
226 MnO_2 ashed samples. The Versapor filters were subse-
227 quently dissolved in a Teflon beaker with a mixture of
228 HNO_3 (ultrapure acid), HF (ultrapure acid), and HClO_4
229 (pure acid) placed on a hot plate. Barium and strontium
230 concentrations were measured at LEGOS by ICP-MS
231 using a Elan 6000 Perkin-Elmer (reproducibility of the
232 method estimated at $\pm 4\%$) using external standards. Na
233 and Ca were analyzed by atomic spectrophotometry at
234 OMP (Observatoire Midi Pyrénées), Toulouse. ^{232}Th was
235 measured by ICP/MS (VG PlasmaQuad II) at the Scottish
236 Universities Research and Reactor Centre, East Kilbride,
237 also using external standards (reproducibility of the meth-
238 od estimated at $\pm 4\%$).

239 Particulate Ba and Ra are mainly associated with barite
240 in the water column (Dehairs et al., 1980, 1990). We calcu-
241 lated excess Ba concentration (Ba_{ex}) and excess Ra activi-
242 ties ($^{226}\text{Ra}_{\text{ex}}$ and $^{228}\text{Ra}_{\text{ex}}$) in suspended particles that refer
243 to the Ba and Ra associated with barite. Ba and Ra concen-
244 trations were corrected for lithogenic fraction using the fol-
245 lowing equations:

$$\text{Ba}_{\text{ex}} = \text{Ba}_{\text{measured}} - ({}^{232}\text{Th}_{\text{measured}} \times [\text{Ba}/{}^{232}\text{Th}]_{\text{upper crust}}), \quad (1) \quad 247$$

$${}^{226}\text{Ra}_{\text{ex}} = {}^{226}\text{Ra}_{\text{measured}} - ({}^{232}\text{Th}_{\text{measured}} \times [{}^{238}\text{U}/{}^{232}\text{Th}]_{\text{upper crust}}), \quad (2) \quad 249$$

$${}^{228}\text{Ra}_{\text{ex}} = {}^{228}\text{Ra}_{\text{measured}} - ({}^{232}\text{Th}_{\text{measured}}), \quad (3) \quad 251$$

252 where $\text{Ba}_{\text{measured}}$, ${}^{226}\text{Ra}_{\text{measured}}$ and ${}^{228}\text{Ra}_{\text{measured}}$ refer to
253 the total concentrations or activities. We used the value
254 of 51.4 (ppm/ppm) for the $[\text{Ba}/{}^{232}\text{Th}]_{\text{upper crust}}$ ratio, which
255 is the mean ratio for the upper crust reported by Taylor
256 and McLennan (1985); ${}^{226}\text{Ra}$ and ${}^{228}\text{Ra}$ activities were cor-
257 rected for the activities in radioactive equilibrium with litho-
258 genic ${}^{238}\text{U}$ and ${}^{232}\text{Th}$, respectively. The ${}^{232}\text{Th}$ activities
259 measured were assumed to be entirely lithogenic. The litho-
260 genic ${}^{238}\text{U}$ activities were estimated from the ${}^{232}\text{Th}$ activi-
261 ties, using the upper continental crust ${}^{238}\text{U}/{}^{232}\text{Th}$ ratio of
262 0.8 (dpm/dpm; Taylor and McLennan, 1985; Anderson
263 et al., 1990). While oceanic particles may often contain
264 an authigenic U fraction, this is assumed to be too recent
265 to be associated with significant ${}^{226}\text{Ra}$ ingrowth. Errors
266 on the excess concentrations were obtained by propagating
267 the errors of each elemental concentrations (Ba, ${}^{226}\text{Ra}$,
268 ${}^{228}\text{Ra}$ as well as ${}^{232}\text{Th}$). It should be stressed here that
269 errors associated with the estimate and the use of mean
270 lithogenic ratios to calculate the lithogenic Ba and Ra

fractions may introduce errors in the calculated excess Ba and Ra concentrations.

As SrSO₄ is the major structural component of acantharians, we measured Sr concentrations in particles to track the presence of acantharians. Sr in particles may also be associated with carbonates. Following Bishop et al. (1977), we estimated non-carbonate Sr concentrations that will be related to acantharians:

$$\text{non-carbonate Sr} = \text{Sr}_{\text{measured}} - (\text{Sr}_{\text{seawater}} + \text{Sr}_{\text{carbonate}}). \quad (4)$$

First, we corrected the Sr concentrations determined from filters collected with in situ pumps for the sea-salt contribution by analyzing the Na content and considering a Sr/Na ratio in seawater of 0.00019 (mol/mol). The Sr content of the carbonate fraction was calculated assuming that carbonates contained 0.17 mol% Sr (Bishop et al., 1977). Carbonate content was estimated from the Ca concentration corrected for (i) the sea-salt contribution (using a Ca/Na ratio of 0.0219 mol/mol in seawater) and (ii) the lithogenic Ca phase using a crustal Ca/Th ratio (ppm/ppm) of 2804 (Taylor and McLennan, 1985). The lithogenic Sr contribution can be neglected. Uncertainty on particulate Sr concentrations is estimated at 10% due to the different corrections (propagation of errors). Again, the use of a mean crustal Ca/Th ratio to calculate the lithogenic Ca may introduce errors in the calculated Ca associated with carbonates. Correction for the Sr associated with sea salt is ca. 35% for most samples but is higher for samples above 200 m (ca. 50%) and reaches 83% for the 20 m pump sample. Sr associated with carbonates represents 15–30% of the total Sr, but is only 3% for sample collected at 20 m.

2.2.3. Sinking particles

Sediment trap samples were first analyzed for Ra isotopes by gamma counting at Modane. Barium and ²³²Th were then measured by instrumental neutron activation (at Laboratoire des Sciences du Climat et de l'Environnement, LSCE, Gif-sur-Yvette, France) for samples collected in 1988–1989 and ICP/MS (Elan 6000 Perkin-Elmer; OMP, Toulouse) for samples collected in 1999–2000. For neutron activation analysis, samples were placed 5 min under a neutron flux of 1.1×10^{14} neutrons cm⁻² s⁻¹ in the Osiris nuclear reactor at Laboratoire Pierre Sûe (Saclay, France). Samples were then measured for their radioactivity using the germanium detectors located at LSCE, Gif-sur-Yvette, France (precision: ±5% estimated from replicate analyses of standards). For ICP/MS measurements, samples were digested in a microwave using a mixture of HF and HNO₃ prior to analysis (precision: ±3% estimated from replicate analyses of standards).

Excess Ba, ²²⁶Ra and ²²⁸Ra were calculated as explained in the suspended particles section. ²²⁸Ra_{ex} activities of sinking particles were also corrected for radioactive decay since the time of sampling (denoted ²²⁸Ra_{ex}^o in Table 3). In contrast, ²²⁸Ra activities of suspended particles and seawater

samples were not decay-corrected because gamma counting of the samples was performed within the 5 months following sample collection.

3. Results

3.1. Hydrography

The vertical structure and circulation of water masses in the region has been previously reviewed by Talley (1996), Joyce and Robbins (1996) and references therein. A CTD profile collected on the OFP cruise (early May 2002) and discrete nutrient data collected on an earlier BATS cruise (mid-April 2002) provided information on vertical structure of water masses that was pertinent to the samples collected (Fig. 1). Below a 30-m surface mixed layer, variable salinity indicated a complex water mass structure within and below the seasonal thermocline, including a distinctive lense of fresher water lying between 160 and 180 m. Subtropical Mode Water (“18 °C water”), which outcrops in the northern Sargasso Sea just south of the Gulf Stream, was found between 275 and 400 m. The depth of the O₂ minimum was 890 m, just above the maxima in AOU, NO₃ and PO₄. An influence of westward spreading Mediterranean water is suggested by positive excursions in salinity and negative excursions in O₂ and PO₄ at depths between 980–1200 and 1300–1470 m. The core of the southward flowing Labrador Sea Water (LSW), a high oxygen and low salinity water mass of $\sigma\theta$ 27.78, was centered at 1650 m, above the North Atlantic Deep Water. Antarctic Bottom Water (AABW), identified by a potential $T < 1.90$ °C and high nutrients, was present below 3800 m.

3.2. Elemental concentrations and ratios

3.2.1. Barium and radium in seawater

Dissolved Ba, ²²⁶Ra and ²²⁸Ra profiles (Fig. 2; Table 1) are similar to those reported earlier for the Atlantic Ocean (Broecker et al., 1967, 1976; Wolgemuth and Broecker, 1970; Kaufman et al., 1973; Chan et al., 1976, 1977; Moore et al., 1985; Kim et al., 2003). Barium concentrations and ²²⁶Ra activities in seawater increase with depth, reflecting uptake during particle formation in shallow waters and subsequent release to the deep water from settling particles. Ba and ²²⁶Ra contents are relatively constant in the upper 400 m (ca. 44.4 nmol kg⁻¹ Ba; ca. 8.6 dpm/100 kg ²²⁶Ra) and increase with increasing water depth. ²²⁶Ra activities increase in two steps to a maximum of 17.5 dpm/100 kg near the seafloor. The steep increase in Ba concentrations and ²²⁶Ra activities below 3700 m can be explained by the presence of Antarctic Bottom Water which are enriched in Ba and ²²⁶Ra (Broecker et al., 1976; Li et al., 1973; Jacques et al., 2004) and by the input of Ba and ²²⁶Ra from the sediments. The ²²⁸Ra activity profile at the OFP site displays a strong vertical gradient from surface to intermediate waters. ²²⁸Ra activities increase again close to the bottom due to diffusion from deep-sea sediments. Calculation

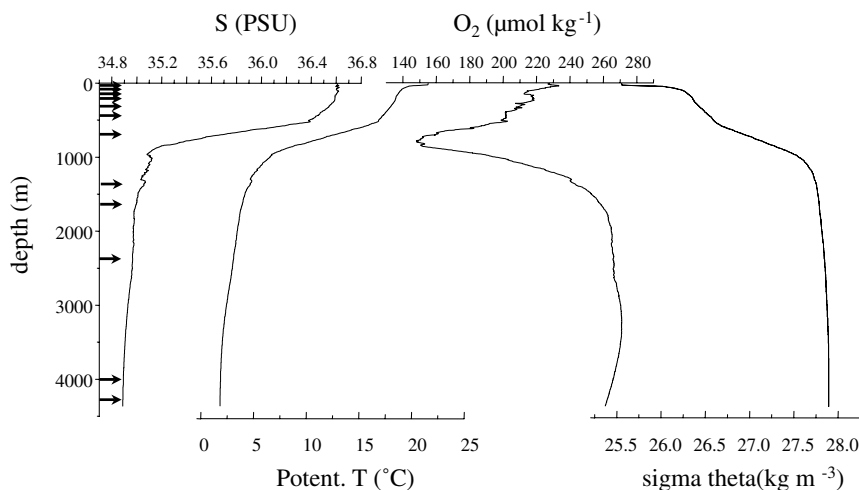


Fig. 1. Hydrography at the OFP site. Profiles of salinity, potential temperature, oxygen and density are reported. Arrows indicate the depths of sample collection (suspended particles and seawater).

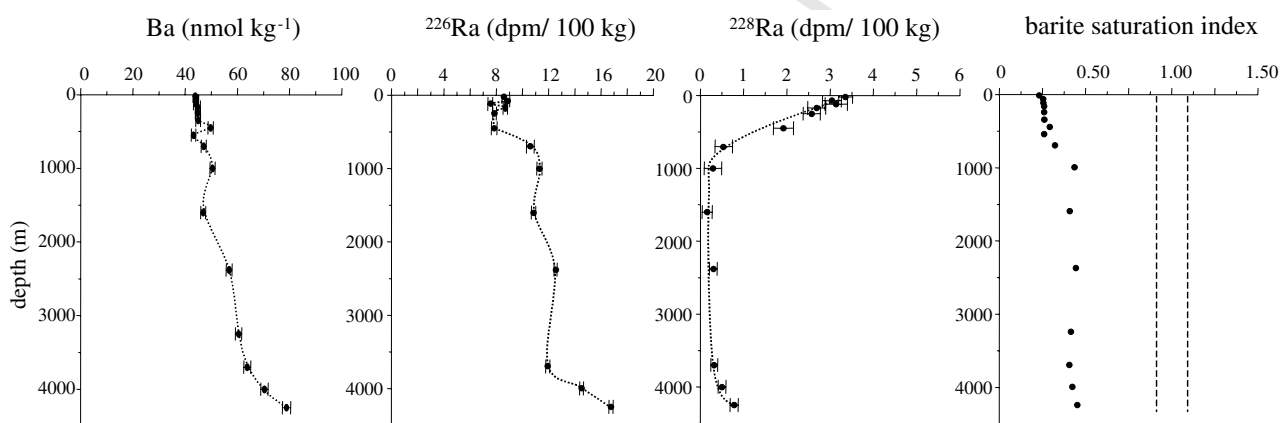


Fig. 2. Dissolved Ba, ^{226}Ra and ^{228}Ra profiles. The barite saturation index profile is also reported. Calculations were made by C. Monnin, LMTG, Toulouse, following Monnin et al. (1999). Pure barite was considered in the calculations. Equilibrium is reached for a saturation index of 1.0 (0.9–1.1). Undersaturation is indicated by a saturation index smaller than 1.0.

Table 1
Results of measurements conducted in seawater

Depth (m)	Ba (nmol kg ⁻¹) (±2%)	^{226}Ra (dpm/100 kg)	^{228}Ra (dpm/100 kg)	$^{228}\text{Ra}/^{226}\text{Ra}$	$^{226}\text{Ra}/\text{Ba}$ (dpm μmol ⁻¹)
20	43.90	8.71 ± 0.12	3.42 ± 0.16	0.39 ± 0.02	1.98 ± 0.05
70	44.32	9.21 ± 0.18	3.16 ± 0.23	0.23 ± 0.03	2.08 ± 0.06
120	44.09	7.82 ± 0.19	3.26 ± 0.27	0.42 ± 0.04	1.77 ± 0.06
170	44.84	8.96 ± 0.17	2.77 ± 0.22	0.31 ± 0.02	2.00 ± 0.06
250	44.80	8.16 ± 0.14	2.67 ± 0.20	0.33 ± 0.03	1.82 ± 0.05
350	45.00				
450	49.80	8.20 ± 0.22	2.01 ± 0.24	0.25 ± 0.03	1.65 ± 0.06
550	43.21				
700	47.12	10.98 ± 0.31	0.56 ± 0.21	0.05 ± 0.02	2.33 ± 0.08
1000	50.52	11.67 ± 0.21	0.30 ± 0.21	0.03 ± 0.02	2.31 ± 0.06
1600	46.92	11.21 ± 0.17	0.16 ± 0.12	0.01 ± 0.01	2.39 ± 0.06
2380	56.87	12.94 ± 0.12	0.31 ± 0.09	0.02 ± 0.01	2.28 ± 0.05
3250	60.48				
3700	63.81	12.49 ± 0.16	0.33 ± 0.08	0.03 ± 0.01	1.96 ± 0.05
4000	70.37	15.20 ± 0.16	0.52 ± 0.09	0.03 ± 0.01	2.16 ± 0.05
4250	78.82	17.50 ± 0.17	0.81 ± 0.09	0.05 ± 0.01	2.22 ± 0.05

377 of the barite saturation index indicates that waters at the
 378 OFP site are undersaturated with respect to barite
 379 (Fig. 2). This pattern agrees with Monnin et al. (1999)
 380 who concluded that the whole Atlantic Ocean was under-
 381 saturated with respect to barite. The barite saturation index
 382 profile suggests that once barite is formed in supersaturated
 383 microenvironments at the OFP site, barite is subject to
 384 dissolution.

385 3.2.2. Barium and radium in suspended particles

386 3.2.2.1. Barium. Particulate barium concentrations are
 387 higher in the upper 1500 m and especially in the upper
 388 500 m (Fig. 3). They are low at 20 m but peak at 70 m

(0.24 nmol kg⁻¹) and 300 m (0.18 nmol kg⁻¹). These con- 389
 390 centrations are in the same range as the values reported
 391 by Bishop (1988) in the Sargasso Sea. They are two orders
 392 of magnitude lower than the dissolved Ba concentrations.
 393 Barite is generally considered the main carrier (Dehairs
 394 et al., 1980, 1990, 1991; Bishop, 1988), with a smaller con-
 395 tribution from lithogenic material. To correct for the latter,
 396 excess Ba concentrations (Ba_{ex}) were calculated by sub-
 397 tracting lithogenic Ba estimated from particulate ²³²Th
 398 concentrations. The lithogenic fraction is relatively small
 399 and constant throughout the water column but increases
 400 sharply below ca. 4000 m, reflecting the presence of a bot-
 401 tom nepheloid layer (Fig. 3; Table 2). Sherrell and Boyle

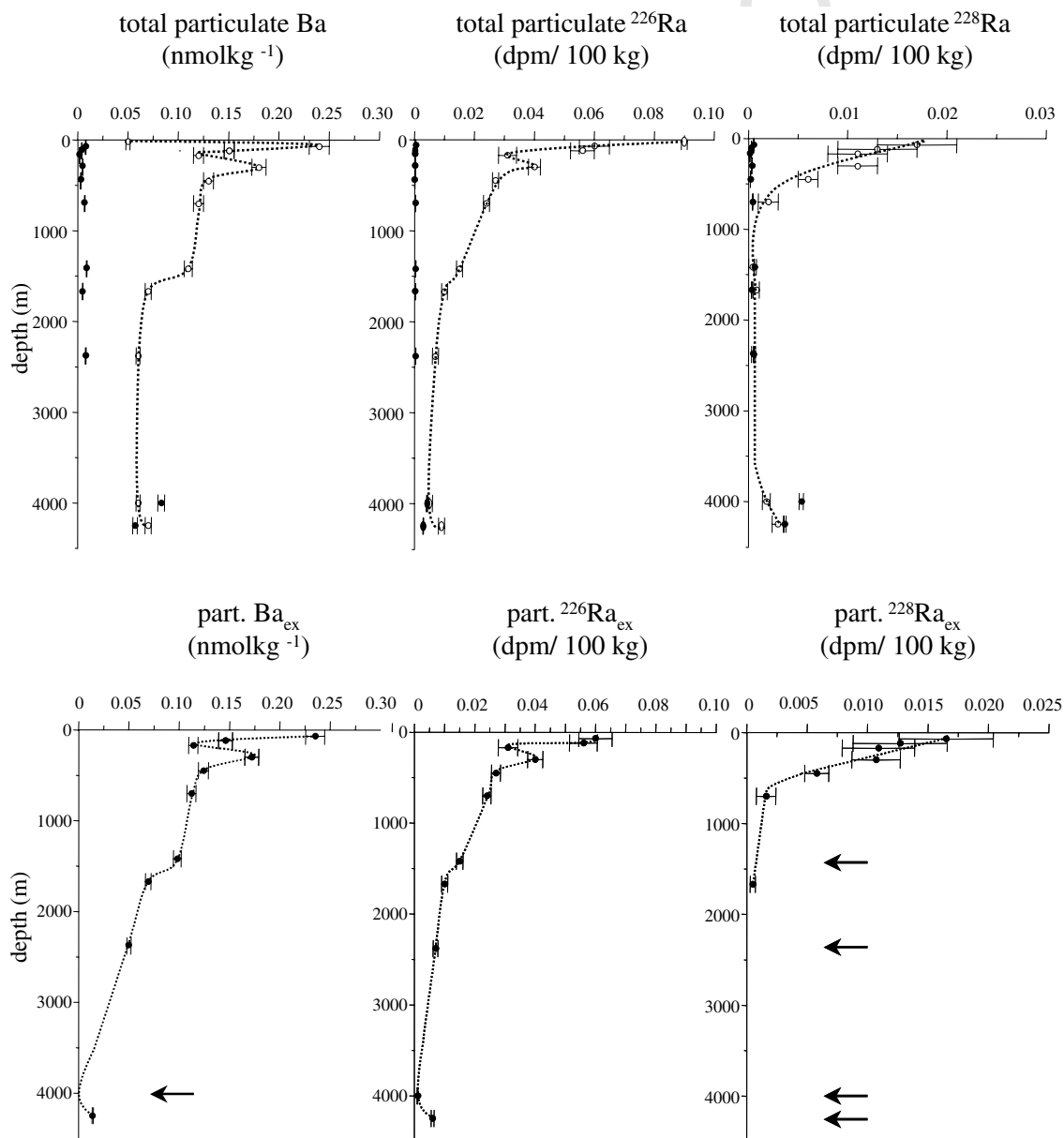


Fig. 3. The upper panels show Ba, ²²⁶Ra and ²²⁸Ra profiles in suspended particles while the lower panels show excess Ba, ²²⁶Ra and ²²⁸Ra profiles in suspended particles (that is, total contents corrected for the lithogenic fraction). In the upper panel, open circles represent total Ba concentrations, total ²²⁶Ra and ²²⁸Ra activities, respectively, whereas solid circles represent the concentrations associated with the lithogenic fraction. Arrows on the lower panel indicate the depths where no significant Ba_{ex} or ²²⁸Ra_{ex} activities were measured in the suspended particles.

Table 2
Results of measurements conducted in suspended particles (in situ pumps)

Depth (m)	^{226}Ra (dpm/100 kg)	^{228}Ra (dpm/100 kg)	^{232}Th (dpm/100 kg) ($\pm 4\%$)	Lithogenic $^{238}\text{U}^a$ (dpm/100 kg) ($\pm 4\%$)	$^{226}\text{Ra}_{\text{ex}}$ (dpm/100 kg)	$^{228}\text{Ra}_{\text{ex}}$ (dpm/100 kg)	$^{228}\text{Ra}_{\text{ex}}/^{226}\text{Ra}_{\text{ex}}$	Ba (nmol kg $^{-1}$) ($\pm 4\%$)	Lithogenic Ba ^b (nmol kg $^{-1}$) ($\pm 4\%$)	Ba _{ex} (nmol kg $^{-1}$) ($\pm 4\%$)	$^{226}\text{Ra}_{\text{ex}}/\text{Ba}_{\text{ex}}$ (dpm μmol^{-1})	Sr ^c (nmol kg $^{-1}$) ($\pm 10\%$)	Non-carbonate Sr ^d (nmol kg $^{-1}$) ($\pm 10\%$)
20	0.090 \pm 0.001	0.0710 \pm 0.0160	n.m.	—	—	—	—	0.048	—	—	—	0.302	0.248
70	0.060 \pm 0.005	0.0170 \pm 0.0040	0.00053	0.00042	0.0165 \pm 0.0035	0.0165 \pm 0.0039	0.276 \pm 0.071	0.243	0.008	0.235	2.54 \pm 0.26	0.508	0.086
120	0.056 \pm 0.004	0.0130 \pm 0.0040	0.00029	0.00023	0.056 \pm 0.0046	0.0127 \pm 0.0039	0.228 \pm 0.073	0.150	0.004	0.146	3.83 \pm 0.35	0.421	0.257
170	0.031 \pm 0.003	0.0110 \pm 0.0030	0.00015	0.00012	0.031 \pm 0.0032	0.0109 \pm 0.003	0.351 \pm 0.104	0.116	0.002	0.114	2.71 \pm 0.30	0.183	0.122
300	0.040 \pm 0.002	0.0110 \pm 0.0020	0.00035	0.00028	0.040 \pm 0.0025	0.0107 \pm 0.0020	0.268 \pm 0.053	0.177	0.005	0.172	2.31 \pm 0.17	0.211	0.128
450	0.027 \pm 0.001	0.0060 \pm 0.0010	0.00021	0.00017	0.027 \pm 0.0015	0.0058 \pm 0.0010	0.216 \pm 0.039	0.127	0.003	0.124	2.17 \pm 0.15	0.164	0.101
700	0.024 \pm 0.001	0.0020 \pm 0.0010	0.00043	0.00034	0.024 \pm 0.0014	0.0016 \pm 0.0008	0.066 \pm 0.034	0.119	0.007	0.112	2.10 \pm 0.15	0.155	0.096
1420	0.015 \pm 0.001	0.0004 \pm 0.0004	0.00058	0.00046	0.015 \pm 0.0011	0	0	0.107	0.009	0.098	1.49 \pm 0.13	0.152	0.088
1670	0.010 \pm 0.001	0.0008 \pm 0.0003	0.00033	0.00026	0.010 \pm 0.0010	0.0005 \pm 0.0002	0.048 \pm 0.019	0.074	0.005	0.069	1.41 \pm 0.16	0.109	0.069
2380	0.007 \pm 0.001	0.0005 \pm 0.0002	0.00053	0.00042	0.007 \pm 0.0008	0	0	0.059	0.008	0.050	1.33 \pm 0.16	0.100	0.058
4000	0.005 \pm 0.001	0.0018 \pm 0.0004	0.00532	0.00425	0.001 \pm 0.0001	0	0	0.057	0.083	0	0	0.102	0.074
4250	0.009 \pm 0.001	0.0030 \pm 0.0006	0.00365	0.00292	0.006 \pm 0.0005	0	0	0.070	0.057	0.014	4.78 \pm 0.41	0.098	0.048

n.m., not measured.

^a Derived from the ^{232}Th activities considering a lithogenic U/Th ratio of 0.8 (dpm/dpm) after Taylor and McLennan (1985).

^b Derived from the ^{232}Th activities using Ba/ ^{232}Th of the upper crust after Taylor and McLennan (1985).

^c Sr content corrected for Sr associated with sea salt.

^d Sr content further corrected for Sr associated with CaCO₃.

(1992) reported a similar increase in particulate Al and Fe concentrations towards the bottom in the water column near Bermuda. Using their Al data and a Ba/Al ratio of 0.0075, we obtain lithogenic Ba concentrations which are in good agreement with our estimates. The lithogenic correction is small in the upper 1500 m and Ba_{ex} concentrations remain high (Fig. 3). In contrast, the Ba content of suspended particles collected in deep waters is dominated by lithogenic Ba, and no Ba_{ex} could be found in the upper nepheloid layer, indicating a substantial decrease in suspended barite concentration with depth. Note that the lithogenic Ba deduced from ^{232}Th concentrations is higher than the Ba content measured in sample collected at 4000 m. Uncertainty associated with the crustal Ba/Th ratio used to calculate the lithogenic Ba may explain such pattern.

3.2.2.2. Radium isotopes. ^{226}Ra activities in suspended particles are highest in surface waters (0.09 dpm/100 kg, i.e., two orders of magnitude lower than the ^{226}Ra activity in seawater) and decrease with depth, with a secondary peak at 300 m (Fig. 3). The excess ^{226}Ra profile is similar to that of excess Ba (Fig. 3). Suspended $^{226}\text{Ra}_{\text{ex}}$ activities are highest in the upper 500 m, where the lowest dissolved ^{226}Ra activities are found (Fig. 2), and decrease with depth before increasing slightly towards the seafloor. Particulate ^{228}Ra activities are also highest towards the surface and decrease rapidly to very low values in mid water. Very little or no excess ^{228}Ra activity remains in suspended particles below 1000 m. For the sample collected at 4000 m, note that the ^{232}Th activity is higher than that of ^{228}Ra .

3.2.3. $^{228}\text{Ra}/^{226}\text{Ra}$ and $^{226}\text{Ra}/\text{Ba}$ ratios in seawater and suspended particles

3.2.3.1. $^{228}\text{Ra}/^{226}\text{Ra}$ ratios. The dissolved $^{228}\text{Ra}/^{226}\text{Ra}$ seawater profile shows a strong vertical gradient in the upper water column as it was observed for the ^{228}Ra activities (Fig. 4). Our data agree with those of Kim et al. (2003) who reported $^{228}\text{Ra}/^{226}\text{Ra}$ ratios from the upper 600 m in the same area. $^{228}\text{Ra}_{\text{ex}}/^{226}\text{Ra}_{\text{ex}}$ activity ratios in suspended particles (Fig. 4 and Table 2) display a profile similar to that of $^{228}\text{Ra}_{\text{ex}}$ activities. $^{228}\text{Ra}_{\text{ex}}/^{226}\text{Ra}_{\text{ex}}$ ratios found in suspended particles match the seawater ratios down to 2000 m depth.

3.2.3.2. $^{226}\text{Ra}/\text{Ba}$ ratios. The dissolved $^{226}\text{Ra}/\text{Ba}$ ratios below 500 m are close to 2.3 dpm μmol^{-1} (that is, the value reported by Chan et al., 1976), which can be considered as a reference value, but we find significantly lower values in the upper 500 m of the water column, above the main thermocline (Fig. 5). $^{226}\text{Ra}_{\text{ex}}/\text{Ba}_{\text{ex}}$ ratios in suspended particles collected in the upper 170 m are higher than 2.3 dpm μmol^{-1} , reaching a maximum (3.8 dpm μmol^{-1}) at 120 m depth (Fig. 5). Such values are higher than the maximum value reported by Moore and Dymond (1991) when analyzing sediment trap material from the Pacific Ocean. Below 120 m, $^{226}\text{Ra}_{\text{ex}}/\text{Ba}_{\text{ex}}$ ratios exhibit a

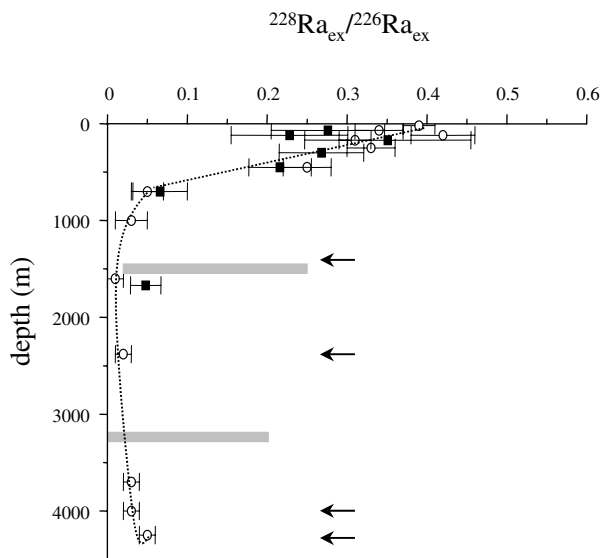


Fig. 4. $^{228}\text{Ra}_{\text{ex}}/^{226}\text{Ra}_{\text{ex}}$ ratios in suspended particles (solid squares) reported together with the ratios found in seawater (open circles). Arrows indicate the depths where no significant $^{228}\text{Ra}_{\text{ex}}$ were measured in the suspended particles. As a comparison, the shaded bars represents the range of values found in sinking particles (at 1500 and 3200 m, respectively).

constant decrease with increasing depth. From 300 to 700 m, $^{226}\text{Ra}_{\text{ex}}/\text{Ba}_{\text{ex}}$ ratios are close to the value of 2.3 $\text{dpm } \mu\text{mol}^{-1}$. Below 1000 m, $^{226}\text{Ra}_{\text{ex}}/\text{Ba}_{\text{ex}}$ ratios are lower, with values as low as 1.33 $\text{dpm } \mu\text{mol}^{-1}$ at 2380 m.

As a comparison, Sr contents were also analyzed in suspended particles. Sr contents are also high in the upper 150 m (Fig. 5). Sr values (total Sr corrected for sea salt as well as non-carbonate Sr) are similar to values reported by Bishop et al. (1977, 1978) who analyzed suspended particles also collected using in situ pumps in the Atlantic Ocean. Maximum non-carbonate Sr concentrations are found at 120 m. Below this depth, non-carbonate Sr con-

centrations decrease with increasing water depth down to ca. 1500 m. Deeper in the water column, Sr contents display constant values.

3.2.4. Ratios in sinking particles (sediment traps)

3.2.4.1. $^{228}\text{Ra}_{\text{ex}}/^{226}\text{Ra}_{\text{ex}}$ ratio. The range of $^{228}\text{Ra}_{\text{ex}}/^{226}\text{Ra}_{\text{ex}}$ ratios found in sinking particles collected during the two different periods is very similar (Fig. 6, Table 3). In most cases, the ratios range between 0.1 and 0.2, with significant variability. Note that for several samples from the deeper sediment trap, no significant excess ^{228}Ra activities could be found. In most cases the ratio found in the deep sediment trap at 3200 m is lower than the ratio found at 1500 m.

3.2.4.2. $^{226}\text{Ra}_{\text{ex}}/\text{Ba}_{\text{ex}}$ ratio. $^{226}\text{Ra}_{\text{ex}}/\text{Ba}_{\text{ex}}$ ratios also display significant variability with time and water depth (0.53–4.09 $\text{dpm } \mu\text{mol}^{-1}$, Fig. 7). In most cases, the $^{226}\text{Ra}_{\text{ex}}/\text{Ba}_{\text{ex}}$ ratio found at 3200 m is lower than the ratio found at 1500 m, with, however, two samples showing the opposite trend (i.e., February–April 1989 and June 2000). Two samples collected at 1500 m in 1988 (i.e., March–May and July–September) display $^{226}\text{Ra}_{\text{ex}}/\text{Ba}_{\text{ex}}$ ratios much higher than the seawater ratio ($>3.5 \text{ dpm } \mu\text{mol}^{-1}$). Sediment trap material from the Pacific Ocean analyzed by Moore and Dymond (1991) did not exhibit such high values. $^{226}\text{Ra}_{\text{ex}}/\text{Ba}_{\text{ex}}$ ratios found in samples collected in 1999–2000 were all $<2.1 \text{ dpm } \mu\text{mol}^{-1}$, with most of the samples displaying ratios lower than the seawater ratios reported in this study ($<1.5 \text{ dpm } \mu\text{mol}^{-1}$).

4. Discussion

4.1. $^{228}\text{Ra}_{\text{ex}}/^{226}\text{Ra}_{\text{ex}}$ ratios

Previous studies have suggested that barite precipitation takes place mainly in the upper 500 m of the water column

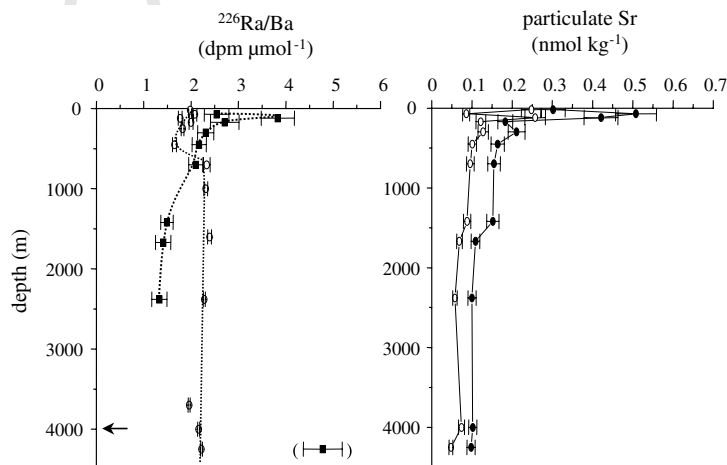


Fig. 5. (Left panel) $^{226}\text{Ra}/\text{Ba}$ ratios in seawater (open circles) reported together with $^{226}\text{Ra}_{\text{ex}}/\text{Ba}_{\text{ex}}$ ratios in suspended particles (closed squares). (Right panel) Sr content measured in suspended particles. Solid circles represent the total Sr content (corrected for the Sr associated with sea salt) while open circles consist in the non-carbonate Sr.

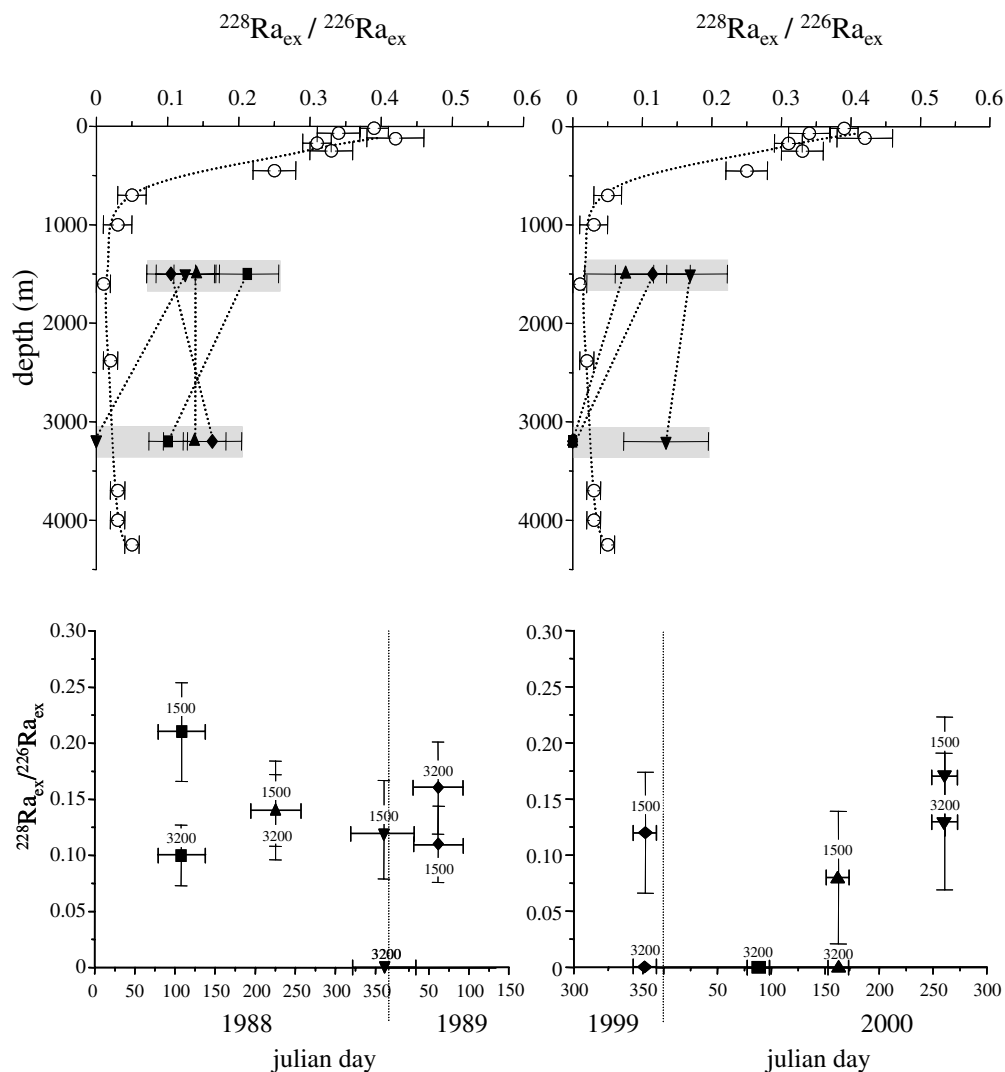


Fig. 6. $^{228}\text{Ra}_{\text{ex}}/^{226}\text{Ra}_{\text{ex}}$ ratios in sinking particles collected with sediment traps reported versus water depth (upper panels) and versus time (lower panels). Solid symbols represent the ratios found in sinking particles whereas open circles represent the seawater ratios obtained during the 2002 cruise. Results obtained on samples collected in 1988–1989 are reported on the left panel, while those from samples collected in 1999–2000 are reported on the right panel. Width of the plots on the lower panels indicates sampling duration. (Left panels) Solid squares: 19 March–17 May 1988 (58 days collection); up triangles: 13 July–13 September 1988 (61 days collection); down triangles: 15 November 1988–1 February 1989 (76 days collection); diamonds: 1 February–4 April 1989 (61 days collection). (Right panels) Diamonds: 10 December 1999–25 December 1999 (15 days collection); solid squares: 23 March 2000–5 April 2000 (14 days collection); up triangles: 5 June 2000–20 June 2000 (15 days collection); down triangles: 5 September 2000–20 September 2000 (15 days collection).

500 (Chow and Goldberg, 1960; Dehairs et al., 1980, 1990,
 501 1991, 1992; Bishop, 1988; Legeleux and Reyss, 1996),
 502 which could account for the higher particulate excess Ba
 503 and ^{226}Ra concentrations found in the upper 500 m at
 504 the OFP site. Suspended barite found deeper in the water
 505 column could have been produced in situ (that is, at the
 506 depth of sample collection) or could have been released
 507 from aggregates settling from shallower depth. When
 508 studying suspended particles in the Sargasso Sea, Bishop
 509 (1988) concluded that barite crystals formed in the
 510 $>53\ \mu\text{m}$ particle size fractions in near-surface waters and
 511 were released into the $1\text{--}53\ \mu\text{m}$ fraction at depths below
 512 the euphotic zone (at 200–300 m). Such release could occur
 513 also deeper in the water column. The decreasing trend in
 514 Ba_{ex} and $^{226}\text{Ra}_{\text{ex}}$ particulate concentrations with depth

(Fig. 3) could thus reflect a decrease in supply of fine barite 515
 crystals by breakdown of settling particles which is expected 516
 to be more intensive in the upper 500 m. Once released 517
 from the supersaturated microenvironments in which they 518
 presumably formed, barite crystals would be subject to dis- 519
 solution in undersaturated waters (Fig. 2; Church and Wol- 520
 gemuth, 1972; Monnin et al., 1999; Rushdi et al., 2000). 521
 Thus, the decrease in particulate Ba_{ex} and $^{226}\text{Ra}_{\text{ex}}$ with 522
 depth could also be partly driven by gradual dissolution 523
 during settling. In addition, barite may also precipitate be- 524
 low 500 m, which would require the presence of supersatu- 525
 rated microenvironments at these depths. The decreasing 526
 trend of Ba_{ex} profile could thus reflect a decrease in the rate 527
 at which barite is produced in situ. With its strong gradient 528
 in the upper water column, the $^{228}\text{Ra}_{\text{ex}}/^{226}\text{Ra}_{\text{ex}}$ of suspend- 529

Table 3
Results of measurements conducted in sinking particles (sediment traps)

Sample	Depth (m)	Sampling duration (d)	Total flux (mg m ⁻² d ⁻¹)	²²⁶ Ra (dpm g ⁻¹)	²²⁸ Ra (dpm g ⁻¹)	²³² Th ^a (dpm g ⁻¹) (±5%)	²³² Th ^b (dpm g ⁻¹) (±3%)	²³⁸ U ^c (dpm g ⁻¹)	²²⁶ Ra _{ex} (dpm g ⁻¹)	²²⁸ Ra _{ex} (dpm g ⁻¹)	²²⁸ Ra ^o _{ex} (dpm g ⁻¹)	²²⁸ Ra ^o _{ex} / ²²⁶ Ra _{ex}	Ba _{ex} (ppm) (±3%)	²²⁶ Ra _{ex} / ²²⁸ Ra _{ex} (dpm μmol ⁻¹)	Ba _{ex} flux (μmol m ⁻² d ⁻¹)
March–May 1988	1500	58	59.8	11.46 ± 0.22	0.79 ± 0.11	0.33	—	0.26	11.20 ± 0.60	0.46 ± 0.07	2.37 ± 0.35	0.21 ± 0.044	433	3.55 ± 0.22	0.19
March–May 1988	3200	58	49.3	8.56 ± 0.17	0.67 ± 0.12	0.51	—	0.41	8.15 ± 0.44	0.16 ± 0.03	0.82 ± 0.15	0.10 ± 0.027	504	2.22 ± 0.14	0.18
July–September 1988	1500	61	31.7	9.30 ± 0.19	0.85 ± 0.13	0.60	—	0.48	8.82 ± 0.48	0.25 ± 0.04	1.24 ± 0.20	0.14 ± 0.032	296	4.09 ± 0.25	0.07
July–September 1988	3200	61	36.4	7.96 ± 0.23	0.77 ± 0.17	0.56	—	0.45	7.51 ± 0.43	0.21 ± 0.05	1.04 ± 0.24	0.14 ± 0.044	799	1.29 ± 0.08	0.21
November 1988–January 1989	1500	76	29.2	10.14 ± 0.23	0.91 ± 0.21	n.m.	0.65	0.52	9.62 ± 0.36	0.26 ± 0.06	1.20 ± 0.28	0.12 ± 0.041	872	0.52 ± 0.07	0.19
November 1988–January 1989	3200	76	37.8	7.66 ± 0.22	0.69 ± 0.2	0.73	—	0.58	7.08 ± 0.41	0	0	0	798	1.22 ± 0.08	0.22
January–April 1989	1500	61	50.9	9.24 ± 0.20	0.77 ± 0.17	0.57	—	0.46	8.78 ± 0.48	0.20 ± 0.05	0.92 ± 0.21	0.11 ± 0.034	716	1.69 ± 0.10	0.27
January–April 1989	3200	61	58.4	7.58 ± 0.15	0.87 ± 0.15	0.62	—	0.50	7.08 ± 0.38	0.25 ± 0.04	1.16 ± 0.21	0.16 ± 0.041	406	2.40 ± 0.15	0.17
December 1999	1500	15	29.7	9.30 ± 0.51	1.28 ± 0.42	—	0.55	0.44	8.86 ± 0.55	0.73 ± 0.24	1.02 ± 0.34	0.12 ± 0.054	908	1.34 ± 0.09	0.20
December 1999	3200	15	24.8	6.76 ± 0.54	0.53 ± 0.25	—	0.81	0.65	6.11 ± 0.52	0	0	0	825	1.02 ± 0.09	0.15
March 2000	1500	14	57.9	7.21 ± 0.41	2.53 ± 0.38	—	n.m.	n.m.	—	—	—	—	—	—	—
March 2000	3200	14	61.2	3.04 ± 0.09	0.57 ± 0.07	—	0.56	0.45	2.59 ± 0.11	0	0	0	666	0.53 ± 0.03	0.30
June 2000	1500	15	28.7	8.13 ± 0.73	1.04 ± 0.57	—	0.58	0.47	7.66 ± 0.73	0.46 ± 0.25	0.58 ± 0.32	0.08 ± 0.059	1042	1.01 ± 0.10	0.22
June 2000	3200	15	19.9	10.10 ± 0.87	0.39 ± 0.28	—	0.64	0.51	9.59 ± 0.87	0	0	0	654	2.01 ± 0.19	0.09
September 2000	1500	15	34.6	6.30 ± 0.29	1.38 ± 0.30	—	0.62	0.50	5.80 ± 0.32	0.76 ± 0.17	0.98 ± 0.22	0.17 ± 0.053	723	0.10 ± 0.07	0.18
September 2000	3200	15	35.1	5.95 ± 0.49	1.23 ± 0.39	—	0.64	0.51	5.44 ± 0.48	0.59 ± 0.19	0.73 ± 0.24	0.13 ± 0.061	719	1.04 ± 0.10	0.18

n.m., not measured.

^a Neutron activation.

^b ICP/MS.

^c Lithogenic ²³⁸U determined from ²³²Th; ±3% for ICP/MS and ±5% for neutron activation.

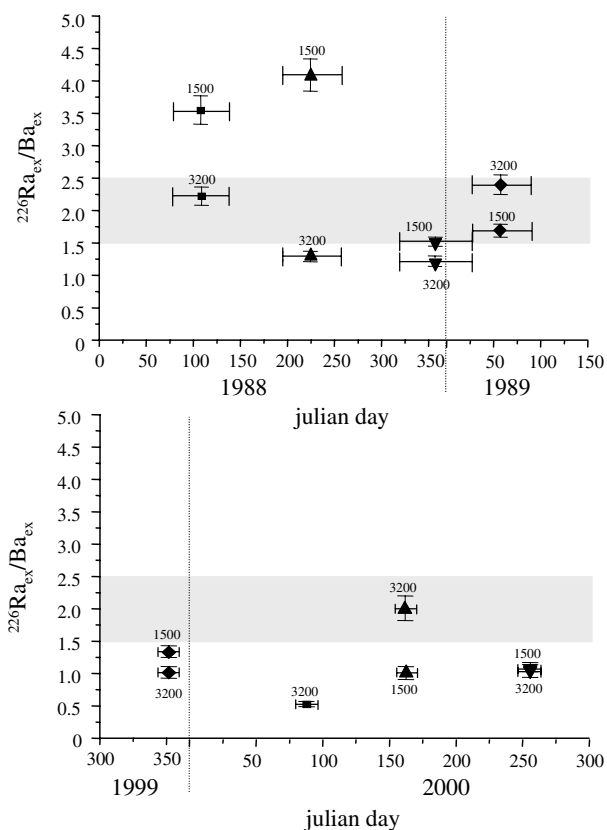


Fig. 7. $^{226}\text{Ra}_{\text{ex}}/\text{Ba}_{\text{ex}}$ ratios in sinking particles reported versus time. The depth of the sediment trap is shown on the plots. Legend is same as Fig. 6. The shaded area represents the range of values found in seawater (Fig. 5). Width of the plots indicates sampling duration.

ed and sinking particles can provide some clarification on the relative importance of these various processes.

4.1.1. $^{228}\text{Ra}_{\text{ex}}/^{226}\text{Ra}_{\text{ex}}$ ratio in suspended particles

When precipitating, barite incorporates radium isotopes from seawater at the depth of formation. Because the $^{228}\text{Ra}/^{226}\text{Ra}$ ratio in seawater displays a strong vertical gradient (Fig. 4), the $^{228}\text{Ra}/^{226}\text{Ra}$ ratio of barite can be used to constrain the depth range of barite formation (Legeleux and Reyss, 1996). Barite forming in the upper water column should have higher $^{228}\text{Ra}/^{226}\text{Ra}$ ratios than barite produced in deeper water. Partial dissolution of settling barite crystals in undersaturated waters is unlikely to affect the $^{228}\text{Ra}/^{226}\text{Ra}$ ratios of barite crystals.

In the upper 500 m, the $^{228}\text{Ra}_{\text{ex}}/^{226}\text{Ra}_{\text{ex}}$ ratios in suspended particles are high (0.22–0.35 dpm/100 kg) and are close to the seawater ratio given for the same water depth (Fig. 4). This pattern agrees with the idea that barite crystals form in the upper water column, as was reported by previous studies (Dehairs et al., 1980, 1990, 1991; Bishop, 1988; Legeleux and Reyss, 1996) and as was suggested by the higher excess Ba concentrations found in this work in the upper 500 m. Deeper in the water column, the $^{228}\text{Ra}_{\text{ex}}/^{226}\text{Ra}_{\text{ex}}$ of suspended particles rapidly decreases to zero below 1000 m.

Suspended particles settle to the seafloor via cycles of aggregation and disaggregation. They sink rapidly (>100 m/day) when incorporated into large sinking particles, and very slowly when released by disaggregation. Their mean sinking rates (300–1000 m/year) have been estimated from measurements of the ^{230}Th in fine suspended particles (Krishnaswami et al., 1981; Bacon and Anderson, 1982; Bacon et al., 1985). If all the suspended Ba_{ex} found in deep water were produced in surface water with a $^{228}\text{Ra}/^{226}\text{Ra}$ of 0.38, we could predict their $^{228}\text{Ra}_{\text{ex}}/^{226}\text{Ra}_{\text{ex}}$ depth profile for a given sinking rate S (Fig. 8):

$$[^{228}\text{Ra}_{\text{ex}}/^{226}\text{Ra}_{\text{ex}}]_z = [^{228}\text{Ra}_{\text{ex}}/^{226}\text{Ra}_{\text{ex}}]_0 \exp(-\lambda_{228}z/S). \quad (5)$$

We also plotted the predicted $^{228}\text{Ra}_{\text{ex}}/^{226}\text{Ra}_{\text{ex}}$ depth profile of suspended particles considering that suspended Ba_{ex} was produced at ~ 250 m with a ratio of 0.30 because it has often been proposed that barite predominantly formed in subsurface (Dehairs et al., 1980, 1990, 1992; Stroobants et al., 1991; Legeleux and Reyss, 1996). Fitting the particulate $^{228}\text{Ra}_{\text{ex}}/^{226}\text{Ra}_{\text{ex}}$ data requires a mean sinking velocity of 40 m/year, which is well below the range of values estimated from particulate ^{230}Th . This observation implies that Ba_{ex} must also be produced in deeper water with lower initial $^{228}\text{Ra}_{\text{ex}}/^{226}\text{Ra}_{\text{ex}}$ ratios. In addition, since the $^{228}\text{Ra}_{\text{ex}}/^{226}\text{Ra}_{\text{ex}}$ of suspended particles is very close (within error bars) to the seawater ratios (Fig. 4), our data suggest very little contribution from aged barite crystals originating from the surface. Transformation during settling may potentially affect the initial $^{228}\text{Ra}/^{226}\text{Ra}$ ratio incorporated by barite in upper waters: recrystallization at depth would thus decrease the $^{228}\text{Ra}/^{226}\text{Ra}$ ratio of settling barite. However, because recrystallization would take place on existing crystals (originating from upper waters), one would expect to find only slight decreases in the $^{228}\text{Ra}/^{226}\text{Ra}$ ratio of settling barite with increasing water depth. In contrast, the $^{228}\text{Ra}_{\text{ex}}/^{226}\text{Ra}_{\text{ex}}$ activity ratios of suspended particles display a large decrease (i.e., from 0.3 to 0.4 in upper waters to <0.05 in intermediate waters). Such a large decrease could be explained by transformation only if the $^{228}\text{Ra}/^{226}\text{Ra}$ signature recorded in upper waters is (almost) entirely replaced by a $^{228}\text{Ra}/^{226}\text{Ra}$ signature recorded deeper in the water column. This scenario would imply significant (i) dissolution of barite formed in surface/subsurface waters and (ii) recrystallization below 500 m, which does not seem too consistent with the recrystallization process (i.e., recrystallisation on existing barite crystals). Therefore, it cannot be excluded that recrystallization contributes to decrease the initial $^{228}\text{Ra}/^{226}\text{Ra}$ ratio of settling barite but it is unlikely to explain the entire decrease found in suspended particles.

We can predict the $^{228}\text{Ra}_{\text{ex}}$ activity profile of suspended particles if all Ba_{ex} was produced in situ (i.e., at the depth of sample collection) from the measured $^{226}\text{Ra}_{\text{ex}}$ activities and the $^{228}\text{Ra}/^{226}\text{Ra}$ ratios of seawater (Fig. 8):

$$\text{Predicted } [^{228}\text{Ra}_{\text{ex}}]_z = \text{Measured } [^{226}\text{Ra}_{\text{ex}}]_z \times \text{Seawater } (^{228}\text{Ra}/^{226}\text{Ra})_z. \quad (6)$$

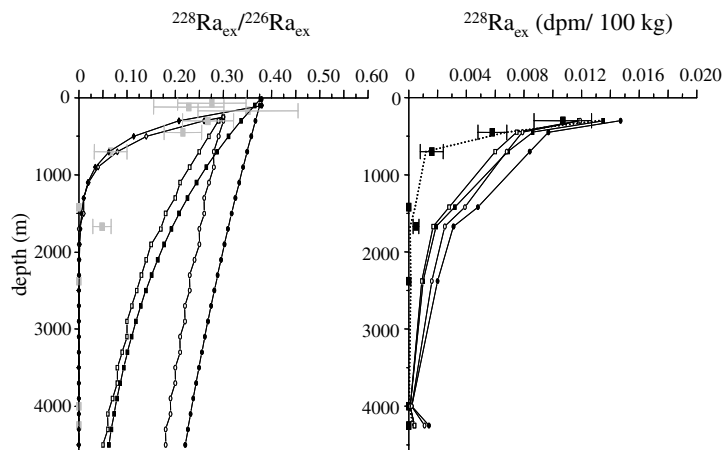


Fig. 8. (Left panel) $^{228}\text{Ra}_{\text{ex}}/^{226}\text{Ra}_{\text{ex}}$ ratio expected in suspended particles considering that the particles acquire the seawater ratio of surface waters (solid symbols; initial ratio of 0.38) or subsurface (open symbols; initial ratio of 0.30) and that they settle at a rate of 1000 m/year (circles), 300 m/year (squares) or 40 m/year (diamonds). Ratios measured in the suspended particles are shown in grey with their associated error bars. (Right panel) $^{228}\text{Ra}_{\text{ex}}$ activities expected in suspended particles collected below 250 m as deduced from the $^{226}\text{Ra}_{\text{ex}}$ activities measured in each sample and considering that the particles acquired the seawater $^{228}\text{Ra}/^{226}\text{Ra}$ ratio in surface waters (solid symbols; initial ratio of 0.38) or subsurface (open symbols; initial ratio of 0.30). Vertical profiles were computed considering settling rates of 300 m/year (squares) and 1000 m/year (circles). The dotted line represents the expected values in case Ba_{ex} incorporates the seawater ratio throughout the water column. $^{228}\text{Ra}_{\text{ex}}$ activities measured in suspended particles are also reported (solid squares with error bars).

610 Similarly, we can predict $^{228}\text{Ra}_{\text{ex}}$ activity profile if all Ba_{ex}
 611 was produced in surface water or subsurface and sinking at
 612 rates S ranging from 300 to 1000 m/year.

$$\begin{aligned} \text{Predicted } [^{228}\text{Ra}_{\text{ex}}]_z &= \text{Measured } [^{226}\text{Ra}_{\text{ex}}]_z \\ &\times \text{Seawater } (^{228}\text{Ra}/^{226}\text{Ra})_0 \\ &\times \exp(-\lambda_{228} z/S). \end{aligned} \quad (7)$$

615 Seawater $(^{228}\text{Ra}/^{226}\text{Ra})_0$ was considered to be 0.38 for surface
 616 waters and 0.30 for subsurface waters.

617 The predictions based on in situ production fall within the
 618 error bars of the data (Fig. 8), confirming that most of the
 619 Ba_{ex} in suspension at depth between 450 and 2380 m is pro-
 620 duced in situ. At 4000 m and below, within the nepheloid
 621 layer, all suspended Ba can be accounted for by lithogenic
 622 material (Fig. 3). These samples appear to be significantly
 623 depleted in ^{228}Ra (i.e., ^{228}Ra activity is lower than ^{232}Th
 624 activity in the same samples), suggesting rapid loss of
 625 ^{228}Ra from resuspended sediment to the water column.

626 Lateral transport of old sediment resuspended from
 627 continental margins to the ocean interior, as suggested by
 628 Moore and Dymond (1991) in the Pacific Ocean, could also
 629 explain the low $^{228}\text{Ra}_{\text{ex}}/^{226}\text{Ra}_{\text{ex}}$ of suspended particles, but
 630 such lateral input would also result in higher suspended
 631 ^{232}Th concentration. The latter is relatively constant in
 632 the upper 2380 m, showing a significant increase only close
 633 to the bottom (Fig. 3; Table 2). The low $^{228}\text{Ra}_{\text{ex}}/^{226}\text{Ra}_{\text{ex}}$ ra-
 634 tios observed between 500 and 2000 m, therefore, are
 635 unlikely to be explained by the lateral transport of particles
 636 resuspended at the continental margins.

637 4.1.2. $^{228}\text{Ra}_{\text{ex}}/^{226}\text{Ra}_{\text{ex}}$ ratio in sinking particles

638 In most cases, the $^{228}\text{Ra}_{\text{ex}}/^{226}\text{Ra}_{\text{ex}}$ ratios found in sink-
 639 ing particles at 1500 and 3200 m are intermediate between

640 that of barite (or particulate Ba_{ex}) originating from surface
 641 or subsurface waters (0.23–0.35) and those formed in deep-
 642 er water (<0.1 ; Fig. 6). These intermediate values suggest
 643 that a significant fraction of the barite intercepted by the
 644 sediment traps originates from the upper water column,
 645 as suggested by Legeux and Reyss (1996), but with equal-
 646 ly significant contributions from deeper waters. The low
 647 $^{228}\text{Ra}/^{226}\text{Ra}$ ratios found in suspended particles at interme-
 648 diate depths suggested that barite could form below 500 m,
 649 presumably in remaining saturated microenvironments.
 650 Such crystals may then be incorporated in the sinking flux.
 651 Recrystallization at depth may not be completely excluded
 652 and could also contribute to lower the $^{228}\text{Ra}/^{226}\text{Ra}$ ratio of
 653 sinking barite.

654 Barite crystals originating from upper waters, which are
 655 not found in the pool of suspended particles below 500 m,
 656 may thus either dissolve in undersaturated waters or be re-
 657 moved from the upper 500 m with the downward flux of
 658 large particles through aggregation processes. Considering
 659 that there is little evidence of barite release from disaggre-
 660 gation of large particles below 500 m (which would increase
 661 $^{228}\text{Ra}_{\text{ex}}/^{226}\text{Ra}_{\text{ex}}$ ratios of suspended particles to values
 662 higher than seawater ratios), it would appear that exchange
 663 of Ba_{ex} between the two pools of particles occurs mainly in
 664 one direction, i.e., large sinking particles entrain barite pro-
 665 duced in deeper water but release little barite to seawater
 666 during settling. This suggests that the increase in seawater
 667 concentration in Ba and ^{226}Ra concentration is mainly
 668 due to vertical diffusion after dissolution on the seafloor,
 669 since dissolution of barite during the short residence time
 670 of large particles in the water column is unlikely to be
 671 significant.

672 There is a relatively large temporal and depth variability
 673 in the $^{228}\text{Ra}_{\text{ex}}/^{226}\text{Ra}_{\text{ex}}$ ratios of the sinking particles. Lege-

leux and Reys (1996) also reported significant fluctuations with time and water depth in the $^{228}\text{Ra}_{\text{ex}}/^{226}\text{Ra}_{\text{ex}}$ ratio of sinking particles collected in the tropical northeast Atlantic (ratios ranging from 0.09 to 0.25 at the oligotrophic site and from 0.09 to 0.30 at the mesotrophic site). Such variability suggests significant temporal variations in the relative proportion of barite originating from surface and intermediate waters, but no pattern could be distinguished which would provide insight into what controls this variability. Mass fluxes and Ba_{ex} fluxes display large variations throughout the year (Table 3; Conte et al., 2001), but no significant correlation could be identified between the $^{228}\text{Ra}_{\text{ex}}/^{226}\text{Ra}_{\text{ex}}$ ratio of sinking particles and any of the downward fluxes (total, organic carbon, silica, carbonates, Ba_{ex}). This may in part be due to the large uncertainties in the ^{228}Ra measurements.

On occasion, $^{228}\text{Ra}_{\text{ex}}$ activity of settling particles drops below detection limits. In particular, this was observed in the sample collected in winter 1988–1989 and in three of the four samples collected during brief (2 weeks) periods in 2000 (Table 3; Fig. 6). In such instances, the intercepted Ba_{ex} could only originate from water deeper than 1000 m, with very little contribution of Ba_{ex} from surface/subsurface waters. Similarly, the addition of barite crystals precipitated below 1500 m to the downward flux could explain the decrease in the $^{228}\text{Ra}_{\text{ex}}/^{226}\text{Ra}_{\text{ex}}$ ratio of sinking particles often observed between 1500 and 3200 m.

4.2. $^{226}\text{Ra}/\text{Ba}$ ratios

The study of $^{226}\text{Ra}_{\text{ex}}/\text{Ba}_{\text{ex}}$ ratios and Sr contents can be used to reinforce our deductions based on $^{228}\text{Ra}/^{226}\text{Ra}$ data and to provide additional information on the possible role of acantharians in barite formation (Bernstein et al., 1987, 1992, 1998).

4.2.1. $^{226}\text{Ra}/\text{Ba}$ ratio in seawater

Earlier studies have indicated that the dissolved $^{226}\text{Ra}/\text{Ba}$ ratios in open ocean waters is generally uniform ($2.3 \text{ dpm } \mu\text{mol}^{-1}$; Chan et al., 1976; Foster et al., 2004). The dissolved $^{226}\text{Ra}/\text{Ba}$ ratios below 500 m agree with this observation, but we find significantly lower values in the upper 500 m of the water column, above the main thermocline (Fig. 5). Similar $^{226}\text{Ra}/\text{Ba}$ profiles have been found at (old) Hale Aloha station off Hawaii and Station K3 in the North-West Pacific (van Beek et al., unpublished data), indicating that this is not a feature unique to the OFP site, and suggesting preferential uptake of Ra over Ba in the upper water column. At similar depths, salinity-normalized Sr concentrations in the Sargasso Sea reported small variations but no clear depletion in surface water which could indicate acantharians production (Mackenzie, 1964; Bernstein et al., 1992, 1998).

4.2.2. $^{226}\text{Ra}_{\text{ex}}/\text{Ba}_{\text{ex}}$ ratio in suspended particles

In the upper 500 m, fractionation during the formation of suspended particulate Ba is corroborated by the high

$^{226}\text{Ra}_{\text{ex}}/\text{Ba}_{\text{ex}}$ ratios of suspended particles compared to seawater at the same depth (Fig. 5). A depth-by-depth correlation between seawater and suspended particles ratios is not warranted because of the different integration times inherent in the data sets: the seawater ratio reflects a longer-term integration whereas the ratio in suspended particles reflects a “snapshot” view. Nonetheless, $^{226}\text{Ra}_{\text{ex}}/\text{Ba}_{\text{ex}}$ ratios are clearly higher than $2.3 \text{ dpm } \mu\text{mol}^{-1}$ in suspended particles collected in the upper 170 m, reaching a maximum ($3.8 \text{ dpm } \mu\text{mol}^{-1}$) at 120 m depth. At the same water depth, a maximum in the non-carbonate Sr contents is observed (Fig. 5).

To a first approximation, suspended Ba_{ex} concentrations determined in this work were attributed to barite. Bernstein et al. (1992, 1998), however, suggested that acantharian skeletons made of celestite (SrSO_4) could play a significant role in the Ba and Ra cycle. Michaels (1988), Michaels et al. (1995) and Bernstein et al. (1992, 1998) reported the presence of abundant acantharian population in the Sargasso Sea. In the present study, we relate the high non-carbonate Sr concentrations in surface waters to acantharian skeletons. Our Sr data agree with the view that acantharians are generally concentrated in surface waters and that their abundance rapidly decreases below 150 m because celestite rapidly dissolves after the death of the organism (Bishop et al., 1977, 1978; Michaels, 1988; Michaels et al., 1995; Bernstein et al., 1992).

The highest $^{226}\text{Ra}_{\text{ex}}/\text{Ba}_{\text{ex}}$ ratio reported at 120 m that corresponds to the maximum in the non-carbonate Sr is likely to be explained by acantharian celestite (Fig. 5). Chemical analogues of strontium, both barium and radium are incorporated into celestite. Based on the solubility products of Ra, Ba and Sr sulfate at 20°C and zero ionic strength, Bernstein et al. (1998) predicted radium enrichments in celestite. The relatively high $^{226}\text{Ra}_{\text{ex}}/\text{Ba}_{\text{ex}}$ ratios and Sr contents in the suspended particles from surface waters therefore likely indicate the presence of acantharians, and their decrease with depth must reflect the dissolution of celestite. We note, however, that even in the non-carbonate Sr maximum (120–170 m), molar $\text{Ba}_{\text{ex}}/\text{Sr}_{\text{ex}}$ ratios remain high (0.6–0.9). This is much higher than the molar Ba/Sr ratio reported for acantharian-derived celestite (3×10^{-3} ; Bernstein et al., 1992). This suggests that particles that carry Ba and Sr at such depths consist in a mixing of acantharians (high Sr content) and barite (high Ba content, which increases the Ba/Sr ratio in the suspended particles). In addition, because celestite dissolves rapidly, sampling of acantharians using in situ pumps is unlikely to be quantitative, which would lower the Sr content determined in the suspended particles. These results suggest that the dissolution of acantharian celestite in upper waters is likely to contribute significantly to barite formation. The resulting barite crystals are expected to incorporate significant amount of Sr, which would increase their solubility. Sr-enriched barite crystals that derive from acantharian celestite in upper waters may thus be more sensitive to dissolution compared with barite

784 crystals that were shown to precipitate deeper in the water
785 column.

786 In the absence of acantharians below 500 m in suspend-
787 ed particles, Ba_{ex} concentrations can be more confidently
788 attributed to barite. In these deeper waters, the $^{226}Ra_{ex}/$
789 Ba_{ex} ratios of suspended particle are lower than those of
790 seawater (Fig. 5) and drop below $2.3 \text{ dpm } \mu\text{mol}^{-1}$, reaching
791 zero at 4000 m before increasing sharply near the seafloor.
792 Moore and Dymond (1991) also found $^{226}Ra_{ex}/Ba_{ex}$ ratios
793 lower than $2.3 \text{ dpm } \mu\text{mol}^{-1}$ in sinking particles from deep
794 Pacific water, which they attributed to presence of old bar-
795 ite crystals (with a low $^{226}Ra/Ba$ ratio) from resuspended
796 margin or deep-sea sediments. Considering the low
797 $^{228}Ra_{ex}/^{226}Ra_{ex}$ ratios and ^{232}Th activities in the suspended
798 particles at OFP, we concluded that barite formed in situ
799 and were not laterally transported. Particulate ratio lower
800 than seawater ratio would imply a preferential uptake of
801 Ba over Ra during barite precipitation. In the upper
802 500 m, a similar fractionation would occur during barite
803 precipitation, but this process would occur in microenvi-
804 ronments enriched in ^{226}Ra by the dissolution of celestite,
805 thereby raising the $^{226}Ra_{ex}/Ba_{ex}$ ratio of particulate Ba
806 (or barite) to values equal or higher to that of ambient sea-
807 water. In the nepheloid layer, Ba_{ex} , Ra_{ex} and Sr_{ex} are small
808 compared to their lithogenic fractions and uncertainties in
809 the lithogenic corrections prevent us to use the excess ratios
810 in a meaningful way.

811 4.2.3. $^{226}Ra_{ex}/Ba_{ex}$ ratio in sinking particles

812 As for $^{228}Ra_{ex}/^{226}Ra_{ex}$, the $^{226}Ra_{ex}/Ba_{ex}$ ratios of sinking
813 particles are intermediate between the ratios measured in
814 shallow and deeper water, confirming the mixed origin of
815 barite or Ba_{ex} intercepted by sediment traps. $^{226}Ra_{ex}/Ba_{ex}$
816 ratios also display significant variability with time and
817 water depth ($0.53\text{--}4.09 \text{ dpm } \mu\text{mol}^{-1}$). With smaller error
818 bars, we can better distinguish the origin of Ba_{ex} in different
819 seasons and years. During the 1988–1989 collection period,
820 the Ba_{ex} intercepted at 1500 m clearly had a predominantly
821 shallow signature (high $^{226}Ra_{ex}/Ba_{ex}$) during Spring and
822 Summer, which is consistent with the $^{228}Ra_{ex}/^{226}Ra_{ex}$ ratios
823 of the same samples when considering the error bars on the
824 latter. On the other hand, the winter samples had a pre-
825 dominantly deep signature. It is not possible, however, to
826 tell from this study whether the two highest $^{226}Ra_{ex}/Ba_{ex}$
827 values $>3.5 \text{ dpm } \mu\text{mol}^{-1}$ are associated with (i) barite crys-
828 tals enriched in ^{226}Ra potentially deriving from the dissolu-
829 tion of acantharians or (ii) acantharian specimens and/or
830 acantharian-derived particles. We note that the highest
831 $^{226}Ra_{ex}/Ba_{ex}$ values are not associated with the highest Sr
832 flux intercepted by the sediment traps (data not shown),
833 as would be expected if the high ratios are associated with
834 acantharian specimen. In addition, observations of Bern-
835 stein et al. (1992) in the Sargasso Sea concluded that
836 acantharian specimen were rare to non-existent at 1500 m
837 depth. However, we agree that this is non-conclusive.

838 In the deep trap, the $^{226}Ra_{ex}/Ba_{ex}$ ratios can more con-
839 fidently be associated with barite as acantharians are not

recovered at such depth (Bernstein et al., 1992). At 840
3200 m, the Spring and Summer samples had lower ratios 841
than at 1500 m, suggesting addition of barite produced be- 842
low 1500 m to the vertical flux. During the 1999–2000 col- 843
lection period, the ratio of most sediment trap samples 844
suggest a predominantly deep origin, as was also suggested 845
by the $^{228}Ra_{ex}/^{226}Ra_{ex}$ ratios. In addition, the $^{226}Ra_{ex}/Ba_{ex}$ 846
ratios lower than the seawater ratio suggest fractionation 847
between Ra and Ba during barite precipitation, a pattern 848
that was also deduced from the ratios of suspended parti- 849
cles. Consequently, ratios found at 3200 m during the 850
two sampling periods suggest that barite (or Ba_{ex}) accumu- 851
lates at the sea-floor with a $^{226}Ra/Ba$ ratio slightly lower 852
than $2.3 \text{ dpm } \mu\text{mol}^{-1}$ (i.e., mean ratio at 3200 m is 853
 $1.5 \text{ dpm } \mu\text{mol}^{-1}$). 854

855 5. Conclusion

Combining measurements of Ba_{ex} , Sr_{ex} , $^{226}Ra_{ex}$ and 856
 $^{228}Ra_{ex}$ in suspended and sinking particles and comparing 857
their $^{228}Ra_{ex}/^{226}Ra_{ex}$ and $^{226}Ra_{ex}/Ba_{ex}$ ratios to those of 858
seawater provide constraints on the origin and mode of for- 859
mation of particulate Ba_{ex} (mostly barite) in the ocean. 860

- 861 $^{228}Ra_{ex}/^{226}Ra_{ex}$ ratios of sinking particles suggest that 862
barite exported to the deep sea has a mixed origin that 863
varies with season. While particles settling to a depth 864
of 1500 m in Spring and Summer can sometimes (but 865
not always) have barite that is predominantly formed 866
in shallow water, in agreement with Legeleux and Reys 867
(1996), barite found in winter samples appear to have 868
been produced in deeper water. At 3200 m, settling parti- 869
cles have generally a larger proportion of barite pro- 870
duced in deep water. Barite production, therefore, is 871
not restricted to shallow water but also seems to be sig- 872
nificant at greater depth. The mechanism postulated by 873
Ganeshram et al. (2003), which invokes uptake of Ba 874
by phytoplankton (with a surface Ra isotopic signature) 875
and subsequent release in microenvironments of sinking 876
particles, would produce a clear surface signal in the bar- 877
ite collected throughout the water column. Our data 878
indicate that this proposed mechanism cannot be the 879
only one that produces barite in the water column. 880
Deeper in the water column, barite must also be pro- 881
duced within microenvironments, which must act as a 882
sink for seawater Ba.
- 883 The $^{228}Ra_{ex}/^{226}Ra_{ex}$ ratios of suspended particles track 884
closely that of seawater, confirming in situ formation 885
of barite in deep water and minimal addition of barite 886
by disaggregation of large sinking particles originating 887
from the overlying mixed layer. The exchange of Ba_{ex} 888
between suspended and sinking particles thus appear 889
to mainly occur through the incorporation of barite pro- 890
duced in deep water into the settling flux.
- 891 The $^{226}Ra_{ex}/Ba_{ex}$ ratio of suspended particles is higher 892
than that of seawater above 200 m and lower below 893
700 m. Suspended particles in the upper water column

894 have also high Sr content indicating the presence of
895 celestite from acantharians. Taken together, these obser-
896 vations suggest (i) significant contribution of celestite
897 dissolution to barite formation in the upper 500 m (ii)
898 preferential precipitation of Ba over Ra during barite
899 formation.

900 4. Regarding implications for paleoceanographic studies,
901 the results reported here indicate that (i) the relationship
902 between barite and productivity is more complex than
903 previously thought (i.e., barite can precipitate deeper
904 than 500 m depth; celestite dissolution may contribute
905 significantly to barite precipitation) and (ii) the elemental
906 and isotopic composition of seawater recorded by
907 barite that accumulates in deep-sea sediments cannot
908 be strictly related to a seawater pattern from the upper
909 500 m of the water column.

911 Acknowledgments

912 We are grateful to the crew and captain of Weatherbird
913 II. We thank Christophe Monnin for the calculation of the
914 Ba saturation index at the OFP site. The manuscript was
915 significantly improved by constructive reviews by three
916 anonymous reviewers and Kelly Falkner, associate editor.
917 We thank Larry Ball and David Schneider at the ICP/
918 MS of WHOI, USA; Valérie Olive at the ICP/MS of East
919 Kilbride, Scotland, UK; Frédéric Candaudap at the ICP/
920 MS of Observatoire Midi Pyrénées, Toulouse; Carole
921 Causserand at the atomic spectrophotometry, Observatoire
922 Midi Pyrénées, Toulouse. We are grateful to John C. We-
923 ber for his help with the sinking particles samples. We also
924 thank Alan Fleer, Susan Brown-Léger and Bernhard Peuc-
925 ker-Ehrenbrink at WHOI. We thank Charlotte Riccio,
926 Thierry Sampieri and Jean-Louis Saury at the underground
927 laboratory of Modane as well as Sophie Ayrault, Serge
928 Boiziau at the Laboratoire Pierre Süe, Saclay. We are
929 grateful to Paul Lethaby and Christine Pequignet (BBSR)
930 for providing the CTD data. This work was supported by
931 a Lavoisier fellowship given by the French Ministry of For-
932 eign Affairs and by the Woods Hole Oceanographic
933 Institution.

934
935 Associate editor: Kelly K. Falkner

936 References

937 Anderson, R.F., Lao, Y., Broecker, W.S., Trumbore, S.E., Hofman,
938 H.J., Wolff, W., 1990. Boundary scavenging in the Pacific Ocean: a
939 comparison of ^{10}Be and ^{231}Pa . *Earth Planet. Sci. Lett.* **96**, 287–304.
940 Bacon, M.P., Anderson, R.F., 1982. Distribution of thorium isotopes
941 between dissolved and particulate forms in the deep sea. *J. Geophys.*
942 *Res.* **87**, 2045–2056.
943 Bacon, M.P., Edmond, J.M., 1972. Barium at GEOSECS III in the
944 Southwest Pacific. *Earth Planet. Sci. Lett.* **16**, 66–74.
945 Bacon, M.P., Huh, C.-A., Fleer, A.P., Deuser, W.G., 1985. Seasonality in
946 the flux of natural radionuclides and plutonium in the deep Sargasso
947 Sea. *Deep-Sea Res. I* **32** (3), 273–286.

Berkman, P.A., Ku, T.-L., 1998. $^{226}\text{Ra}/\text{Ba}$ ratios for dating Holocene
948 biogenic carbonates in the Southern Ocean: preliminary evidence from
949 Antarctic coastal mollusc shells. *Chem. Geol.* **144**, 331–334.
950 Bernstein, R.E., Byrne, R.H., 2004. Acantharians and marine barite. *Mar.*
951 *Chem.* **86**, 45–50.
952 Bernstein, R.E., Betzer, P.R., Feely, R.A., Byrne, R.H., Lamb, M.F.,
953 Michaels, A.F., 1987. Acantharian fluxes and strontium to chlorinity
954 ratios in the North Pacific Ocean. *Science* **237**, 1490–1494.
955 Bernstein, R.E., Byrne, R.H., Betzer, P.R., Greco, A.M., 1992. Morphol-
956 ogies and transformations of celestite in seawater: the role of
957 acantharians in strontium and barium geochemistry. *Geochim. Cos-*
958 *mochim. Acta* **56**, 3273–3279.
959 Bernstein, R.E., Byrne, R.H., Schijf, J., 1998. Acantharians: a missing link
960 in the oceanic biogeochemistry of barium. *Deep-Sea Res. II* **45**, 491–
961 505.
962 Bishop, J.K.B., 1988. The barite–opal–organic carbon association in
963 oceanic particulate matter. *Nature* **332**, 341–343.
964 Bishop, J.K.B., Edmond, J.M., Ketten, D.R., Bacon, M.P., Silker, W.B.,
965 1977. The chemistry, biology, and vertical flux of particulate matter
966 from the upper 400 m of the equatorial Atlantic Ocean. *Deep-Sea Res.*
967 **24**, 511–548.
968 Bishop, J.K.B., Ketten, D.R., Edmond, J.M., 1978. The chemistry,
969 biology, and vertical flux of particulate matter from the upper 400 m of
970 the Cape Basin in the southeast Atlantic Ocean. *Deep-Sea Res.* **25**,
971 1121–1161.
972 Broecker, W.S., Li, Y.H., Cromwell, J., 1967. Radium-226 and Radon-
973 222: concentration in Atlantic and Pacific Oceans. *Science* **158**, 1307–
974 1310.
975 Broecker, W.S., Goddard, J., Sarmiento, J.L., 1976. The distribution of
976 ^{226}Ra in the Atlantic Ocean. *Earth Planet. Sci. Lett.* **32**, 220–235.
977 Chan, L.H., Edmond, J.M., Stallard, R.F., Broecker, W.S., Chung, Y.C.,
978 Weiss, R.F., Ku, T.L., 1976. Radium and barium at GEOSECS
979 stations in the Atlantic and Pacific. *Earth Planet. Sci. Lett.* **32**, 258–
980 267.
981 Chan, L.H., Drummond, D., Edmond, J.M., Grant, B., 1977. On the
982 barium data from the Atlantic GEOSECS expedition. *Deep-Sea Res.*
983 **24**, 613–649.
984 Chow, T.J., Goldberg, E.D., 1960. On the marine geochemistry of barium.
985 *Geochim. Cosmochim. Acta* **20**, 192–198.
986 Chung, Y.-C., 1974. Radium-226 and Ra–Ba relationships in Antarctic
987 and Pacific waters. *Earth Planet. Sci. Lett.* **23**, 125–135.
988 Chung, Y.-C., 1976. A deep ^{226}Ra maximum in the northeast Pacific.
989 *Earth Planet. Sci. Lett.* **32**, 249–257.
990 Chung, Y.-C., Craig, H., 1980. ^{226}Ra in the Pacific Ocean. *Earth Planet.*
991 *Sci. Lett.* **49**, 267–292.
992 Church, T.M., Wolgemuth, K., 1972. Marine barite saturation. *Earth*
993 *Planet. Sci. Lett.* **15**, 35–44.
994 Conte, M.H., Ralph, N., Ross, E.H., 2001. Seasonal and interannual
995 variability in deep ocean particles fluxes at the Oceanic Flux Program
996 (OFP)/Bermuda Atlantic Time Series (BATS) site in the western
997 Sargasso Sea near Bermuda. *Deep-Sea Res.* **48**, 1471–1505.
998 Dehairs, F., Chesselet, R., Jedwab, J., 1980. Discrete suspended particles
999 of barite and the barium cycle in the open ocean. *Earth Planet. Sci.*
1000 *Lett.* **49**, 528–550.
1001 Dehairs, F., Goeyens, L., Stroobants, N., Bernard, P., Goyet, C., Poisson,
1002 A., Chesselet, R., 1990. On suspended barite and the oxygen minimum
1003 in the Southern Ocean. *Global Biogeochem. Cycles* **4** (1), 85–102.
1004 Dehairs, F., Stroobants, N., Goeyens, L., 1991. Suspended barite as tracer
1005 of biological activity in the Southern Ocean. *Mar. Chem.* **35**, 399–410.
1006 Dehairs, F., Baeyens, W., Goeyens, L., 1992. Accumulation of suspended
1007 barite at mesopelagic depths and export production in the Southern
1008 Ocean. *Science* **258**, 1332–1335.
1009 Dickey, T., Zedler, S., Frye, D., Jannasch, H., Manov, D., Sigurdson, D.,
1010 McNeil, J.D., Dobeck, L., Yu, X., Gilboy, T., Bravo, C., Doney, S.C.,
1011 Siegel, D.A., Nelson, N., 2001. Physical and biogeochemical variability
1012 from hours to years at the Bermuda Testbed Mooring site: June 1994–
1013 March 1998. *Deep-Sea Res. II* **48**, 2105–2140.
1014

- 1015 Dymond, J., Suess, E., Lyle, M., 1992. Barium in deep-sea sediment: a
1016 geochemical proxy for paleoproductivity. *Paleoceanography* **7** (2), 163–
1017 181.
- 1018 Foster, D.A., Staubwasser, M., Henderson, G.M., 2004. ^{226}Ra and Ba
1019 concentrations in the Ross Sea measured with multicollector ICP mass
1020 spectrometry. *Mar. Chem.* **87**, 59–71.
- 1021 François, R., Honjo, S., Manganini, S.J., Ravizza, G.E., 1995. Biogenic
1022 barium fluxes to the deep sea: implications for paleoproductivity
1023 reconstruction. *Global Biogeochem. Cycles* **9** (2), 289–303.
- 1024 Ganeshram, R.S., François, R., Commeau, J., Brown-Leger, S.L., 2003.
1025 An experimental investigation of barite formation in seawater.
1026 *Geochim. Cosmochim. Acta* **67** (14), 2599–2605.
- 1027 Gingele, F., Dahmke, A., 1994. Discrete barite particles and barium as
1028 tracers of paleoproductivity in South Atlantic sediments. *Paleocea-
1029 nography* **9** (1), 151–168.
- 1030 Jacquet, S.H.M., Dehairs, F., Rintoul, S., 2004. A high resolution transect
1031 of dissolved barium in the Southern Ocean. *Geophys. Res. Lett.* **31**,
1032 L14301. doi:10.1029/2004GL020016.
- 1033 Joyce, T.M., Robbins, P., 1996. The long-term hydrographic record at
1034 Bermuda. *J. Climate* **9**, 3121–3131.
- 1035 Kaufman, A., Trier, R.M., Broecker, W.S., Feely, H.W., 1973.
1036 Distribution of ^{228}Ra in the world ocean. *J. Geophys. Res.* **78**
1037 (36), 8827–8848.
- 1038 Kim, G., Hussein, N., Church, T., 2003. Tracing the advection of organic
1039 carbon into the subsurface Sargasso Sea using $^{228}\text{Ra}/^{226}\text{Ra}$ tracer.
1040 *Geophys. Res. Lett.* **30** (16), 1874. doi:10.1029/2003GL017565.
- 1041 Krishnaswami, S., Sarin, M.M., Somayajulu, B.L.K., 1981. Chemical and
1042 radiochemical investigations of surface and deep particles in the Indian
1043 Ocean. *Earth Planet. Sci. Lett.* **54**, 81–96.
- 1044 Ku, T.-L., Lin, M.-C., 1976. ^{226}Ra distribution in the Antarctic Ocean.
1045 *Earth Planet. Sci. Lett.* **32**, 236–248.
- 1046 Ku, T.-L., Huh, C.-A., Chen, P.S., 1980. Meridional distribution of ^{226}Ra
1047 in the eastern Pacific along GEOSECS cruise tracks. *Earth Planet. Sci.
1048 Lett.* **49**, 293–308.
- 1049 Legeleux, F., Reyss, J.-L., 1996. Ra-228/Ra-226 activity ratio in oceanic
1050 settling particles: Implications regarding the use of barium as a proxy
1051 for paleoproductivity reconstruction. *Deep-Sea Res. I* **43** (11–12),
1052 1857–1863.
- 1053 Li, Y.H., Ku, T.L., Mathieu, G.G., Wolgemuth, K., 1973. Barium in the
1054 Antarctic Ocean and implications regarding the marine Geochemistry
1055 of Ba and ^{226}Ra . *Earth Planet. Sci. Lett.* **19**, 352–358.
- 1056 Li, Y.H., Feely, H.W., Toggweiler, J.R., 1980. ^{228}Ra and ^{228}Th concen-
1057 trations in GEOSECS Atlantic surface waters. *Deep-Sea Res.* **27A**,
1058 545–555.
- 1059 Mackenzie, F.T., 1964. Strontium content and variable strontium-
1060 chlorinity relationship of Sargasso Sea water. *Science* **146**, 517–518.
- 1061 Michaels, A.F., 1988. Vertical distribution and abundance of Acantharia
1062 and their symbionts. *Mar. Biol.* **97**, 559–569.
- 1063 Michaels, A.F., Caron, D.A., Swanberg, N.R., Howse, F.A., Michaels, C.,
1064 1995. Planktonic sarcodines (Acantharia, Radiolaria, Foraminifera) in
1065 surface waters near Bermuda: abundance, biomass and vertical flux. *J.
1066 Plankton Res.* **17** (1), 131–163.
- 1067 Monnin, C., Jeandel, C., Cattaldo, T., Dehairs, F., 1999. The marine
1068 barite saturation state of the world's oceans. *Mar. Chem.* **65**, 253–261.
- 1069 Moore, W.S., 1987. Radium 228 in the South Atlantic Bight. *J. Geophys.
1070 Res.* **92**, 5177–5190.
- Moore, W.S., Dymond, J., 1991. Fluxes of Ra-226 and barium in the
Pacific Ocean: the importance of boundary processes. *Earth Planet.
Sci. Lett.* **107**, 55–68.
- Moore, W.S., Reid, D.F., 1973. Extraction of radium from natural waters
using manganese-impregnated acrylic fibers. *J. Geophys. Res.* **78**, 8880–
8886.
- Moore, W.S., Key, R.M., Sarmiento, J.L., 1985. Techniques for precise
mapping of ^{226}Ra and ^{228}Ra in the ocean. *J. Geophys. Res.* **90**, 6983–
6995.
- Nürnberg, C.C., Bohrmann, G., Schlüter, M., 1997. Barium accumulation
in the Atlantic sector of the Southern Ocean: results from 190,000-year
records. *Paleoceanography* **12** (4), 594–603.
- Paytan, A., Kastner, M., Chavez, F.P., 1996a. Glacial to Interglacial
fluctuations in productivity in the equatorial Pacific as indicated by
marine barite. *Science* **274**, 1355–1357.
- Paytan, A., Moore, W.S., Kastner, M., 1996b. Sedimentation rate as
determined by ^{226}Ra activity in marine barite. *Geochim. Cosmochim.
Acta* **60** (22), 4313–4319.
- Reyss, J.-L., Schmidt, S., Legeleux, F., Bonte, P., 1995. Large, low
background well-type detectors for measurements of environmental
radioactivity. *Nucl. Instrum. Methods A* **357**, 391–397.
- Rhein, M., Schlitzer, R., 1988. Radium-226 and barium sources in the
deep East Atlantic. *Deep-Sea Res.* **35** (9), 1499–1510.
- Rushdi, A., McManus, J., Collier, R., 2000. Marine barite and celestite
saturation in seawater. *Mar. Chem.* **69**, 19–31.
- Schmitz, B., 1987. Barium, equatorial high productivity, and the northward
wandering of the Indian continent. *Paleoceanography* **2** (1), 63–77.
- Sherrell, R.M., Boyle, E.A., 1992. The trace metal composition of
suspended particles in the oceanic water column near Bermuda. *Earth
Planet. Sci. Lett.* **111**, 155–174.
- Stroobants, N., Dehairs, F., Goeyens, L., Vanderheijden, N., van Grieken,
R., 1991. Barite formation in the Southern Ocean water column. *Mar.
Chem.* **35**, 411–421.
- Staubwasser, M., Henderson, G.M., Berkman, P.A., Hall, B.L., 2004. Ba,
Ra, Th, and U in marine mollusc shells and the potential of $^{226}\text{Ra}/\text{Ba}$
dating of Holocene marine carbonate shells. *Geochim. Cosmochim.
Acta* **68** (1), 89–100.
- Steinberg, D.K., Carlson, C.A., Bates, N.R., Johnson, R.J., Michaels,
A.F., Knap, A.H., 2001. Overview of the U.S. JGOFS Bermuda
Atlantic Time-Series Study (BATS): a decade look at ocean biology
and biogeochemistry. *Deep-Sea Res.* **48**, 1405–1448.
- Talley, L., 1996. North Atlantic circulation and variability, reviewed for
the CNLS conference. *Physica D*, 625–646.
- Taylor, S.R., McLennan, S.M., 1985. *The Continental Crust: Its Compo-
sition and Evolution*. Blackwell, Cambridge, MA.
- van Beek, P., Reyss, J.-L., 2001. ^{226}Ra in marine barite: new constraints on
supported ^{226}Ra . *Earth Planet. Sci. Lett.* **187**, 147–161.
- van Beek, P., Reyss, J.-L., Gersonde, R., Paterne, M., Rutgers van der
Loeff, M., Kuhn, G., 2002. ^{226}Ra in barite: absolute dating of
Holocene Southern Ocean sediments and reconstruction of sea-surface
reservoir ages. *Geology* **30** (8), 731–734.
- van Beek, P., Reyss, J.-L., DeMaster, D., Paterne, M., 2004. ^{226}Ra -in
marine barite: relationship with carbonate dissolution and sediment
focusing in the equatorial Pacific. *Deep-Sea Res. I* **51**, 235–261.
- Wolgemuth, K., Broecker, W.S., 1970. Barium in sea water. *Earth Planet.
Sci. Lett.* **8**, 372–378.